NATIONAL TRANSPORTATION SAFETY BOARD

Office of Research and Engineering
Materials Laboratory Division
Washington, D.C. 20594

November 16, 2017

MATERIALS LABORATORY FACTUAL REPORT Report No. 17-050

1. ACCIDENT

Place : Graettinger, Iowa
Date : March 10, 2017
Vehicle : Union Pacific Ethanol Unit Train, UEGKOT-09
NTSB No. : DCA17MR007
Investigator : Michael Hiller, RPH-10

2. COMPONENTS EXAMINED

Sections of 90-lb. rail track

3. DETAILS OF THE EXAMINATION

On Friday, March 10, 2017, about 12:50 am central standard time, an eastbound Union Pacific (UP) unit ethanol train derailed near milepost 56.8 at a railroad bridge near Graettinger, IA (see Figure 1).[1] The train was powered by three locomotives, with 98 loaded tank cars and two buffer cars. Twenty loaded tank cars in positions 21 through 40 derailed. Fourteen of the derailed tank cars released over 300000 gallons of undenatured ethanol, fueling a post-accident fire. Approximately 400 feet of rail and the 152-foot timber rail bridge were destroyed in the accident.

3.1 Initial On-Scene Examination of Accident Track

This portion of the Union Pacific Railroad track was categorized under the Estherville subdivision, consisting of a single main track between milepost 0.0 and milepost 79.3. The track recovered at the site of the derailment was classified as Class 3 track consisting of 90-pound rail, having a tangent track alignment (straight with no curves).[2] Figure 2 illustrates the general alignment of the track and timber bridge at the derailment location.

The crossties measured 9 inches by 7 inches in cross section and 8.5 feet long, spaced 19.5 inches on center (nominal). The crossties were box anchored with rail anchors

[1] Union Pacific Railroad (UP) is a freight hauling railroad headquartered in Omaha, NE that states they operates 32100 route miles of track in the United States.
[2] As defined by the Federal Railroad Administration (FRA), Class 3 track has a maximum operating speed of 40 mph for freight and 60 mph for passenger. However at the time of the accident, UP restricted freight train speeds in this subdivision to 30 mph or lower and does not operate passenger service in this subdivision. Ninety-pound (90-lb.) rail is track that weighs approximately 90 pounds per yard of length.

every other tie to restrain longitudinal movement of the continuously-welded rail (CWR). The rail was seated in ten-inch single shoulder tie plates that lay between the bottom surface of the rail and the top surface of timber crossties. The rail was fastened through the tie plates to standard wooden crossties with conventional six inch cut track spikes. The spiking pattern used by UP prior to the derailment consisted of one rail-holding spike on the gage side and one rail-holding spike on the field side.

The track was supported by ballast consisting of a granite and limestone rock mixture. During the on-scene portion of the investigation, the ballast was estimated to be a minimum of 8 to 12 inches deep beneath the crossties. This ballast depth was estimated for material located outside of the portion disturbed by the derailment.

According to UP documentation, on average, one train consist passed through the subdivision every other day. According to records provided by UP, the 2016 total tonnage passing through the main track between milepost 48.49 and milepost 70.56 was documented at 2.4 million gross tons. This section of track was last tied and surfaced in 1987.

The on-scene investigation primarily concerned the recovery, identification, and reconstruction of the rail that was displaced by the derailment. For the purposes of this investigation, the recovered track was organized into “north rail” and “south rail.” As shown in Figure 2, this nomenclature describes the general position of each piece of track, with the general eastward direction traveled by the train.

The total displaced rail measured about 400 feet on both the north rail and south rails. The on-scene group recovered approximately 391 feet of the north rail and approximately 385 feet of the south rail. This rail was identified by the manufacturer, manufacture dates, and rail fracture characteristics. The north and south rail pieces were labeled in sequential order, starting from the westernmost torch cuts and progressing through the accident area. Figure 3 illustrates a typical portion of the track reconstruction on scene. Figure 4 shows the general layout of the track survey measurements, showing length of track between the torch cuts ends of the rail on either side of the derailment location.

The recovered inventory of the rail found on scene is documented in Table I for the north rail and Table II for the south rail. These tables detail the nomenclature for each rail piece, as identified on scene, and the length of each piece measured on scene. The tables also contain the cumulative length of all the recovered rail, measured from the west torch cut end of pieces 0N and 0S, respectively. It should be noted that, in part due to different lengths, the fragments numbered on the north and south rail do not necessarily correlate. For example, pieces 9N and 9S were not across from each other.

To accurately arrange the fractured pieces in the order present at the time of the derailment, these pieces were compared with those in documentation from UP on the Esterville Subdivision rail makeup. These records describe the location of plant welds (PW)

in the rail.[3] As such, both Table I and Table II show locations of the plant weld(s) and the length from each recorded weld, in feet, where applicable.

Figure 5 and Figure 6 show lengthwise representations of these tabulated recovered rail pieces, as labeled at the investigation site, with the lengths relative to scale. The figures show the north and south rail representations, respectively. With the north rail depicted in Figure 5, the observed locations of the welds on the recovered pieces were compared and matched to the recorded welds provided in documentation from UP. There were no supplied records for the south rail. Approximate locations of the west and east headwalls of the former timber bridge are identified on these figures.

The location of the welds on the reconstructed rail were generally consistent with the locations on the track documentation. However, some of the plant welds found on-scene were not noted in the supplied records. The comparison of the welds suggested that the missing rail pieces would not have contained welds. However, the overall spacing of the welds was inconsistent with 8N to 12N being located east of pieces 13N through 16N (as shown in the drawing).

The condition of the west- and east-facing ends of the recovered rail pieces are described in the tables. Most of the fractured rail pieces exhibited features consistent with overstress fracture—these fractured ends are not specifically labeled in the tables. Many of the pieces were sectioned using either a cutting torch or a mechanical saw—these cut ends are labeled as “torch cut” or “saw cut”, respectively.

Many of the recovered rail pieces on scene exhibited prominent features, which are noted in Table I and Table II. The features noted in the tables include rail batter (labeled as either RB and LB), head checking (HC), wheel flange elevation (riding up), flakes, split webs, fire deposits, and recovery breaks. These features were consistent with damage typical of a loaded freight train derailment.

Rail batter, as shown in Figure 7, is indicative of rail-wheel impact that occurs after a rail has broken. In the Table I and Table II, the rail batter is described either receiving batter or leaving batter (RB and LB, respectively), and is classified as heavy or minimal, depending on the relative depth and length of damage. Figure 7 also shows head checking (HC) on the gage side.[4] The head checking was severe enough that it developed into flakes on the gage side of the head.[5] Figure 8 shows another example of head checking and surface flaking, consistent with rolling contact fatigue due to wheel-rail interaction.

The west side of the rail piece 4S exhibited a split web (see Figure 9). A split web is a fracture parallel to the rolling direction of the rail located along the web. In this case, the

[3] Plant welds are butt welds joining two pieces of rail, that are welded off-site before being joined to the main track.
[4] Head checking is a transverse surface cracking (perpendicular to the rail running direction) on the gage corner of rail heads resulting from severe cold working of the surface material due to wheel-rail interaction.
[5] Flaking in rail heads is a progressive horizontal separation of the running surface of the rail near the gage corner, manifesting as shallow slivers, chips, or scales.

fracture was saw-toothed, consistent with overstress failure in shear across a thin wall. This piece was also a "plug rail," in that it was installed after the last full installation of the track at the accident site.

Figure 10 shows multiple pieces that separated due to a compound fractures. Fractures for these pieces were oriented in the transverse and longitudinal directions, present in the head, web, and base of the rail.

Figure 11 shows a piece that exhibited a reddish-orange colored compounds. As there were no coatings on the rail, and as the compounds were also present on the fracture surfaces, the material was consistent with post-derailment contamination. The likely source would be the fire-fighting compounds used during the post-accident pool fire of released ethanol. These compounds would not have been present during or a factor in the derailment.

A "recovery break" was an artifact where a fracture occurred in a piece during the recovery and reconstruction on site during the post-accident investigation. This occurred between pieces 24N and 25N, and was later found to have occurred in 10N and 11N.

3.2 Visual Examination of Selected Rail Pieces

Several pieces of rail from the derailment site were sent to the NTSB Materials Laboratory for group examination. From the north rail, those pieces were 10N, 11N, 12N, 13N, 14N, 15N (2 pieces), 16N, and 17N. From the south rail, the pieces sent were 4S, 5S, and 10S, with sections of 3S and 6S torch cut away from the larger fragments.

3.2.1 Initial Non-Destructive Testing and Visual Observations.

Several of the pieces were examined using ultrasonic testing, performed by UP personnel, certified ASNT Level II.[6] This testing was performed using a 70° transducer at 2.25 MHz, with a reference gain of 64 dB. The transducer was applied to the running surfaces of the rail heads with a hydrophilic couplant. No crack indications were detected from ultrasonic inspection of the rail heads, which was consistent with previous field inspection data of the track prior to derailment.

The transverse head profiles of several of the rail fragments were examined using a MiniProf Rail stylus tool.[7] The rail heads examined were 10N, 12N, 14N and 10N. The processed data from these head profiles are shown in Figure 12 through Figure 15, respectively.

Further photographic documentation of rail pieces 4S, 10S, 10N, 11N, and 12N was performed and is shown in Figure 16 through Figure 34. For the south fragment, the field

[6] The American Society for the Nondestructive Testing (ASNT) is an international technical society that produces standards for qualification and certification of personnel in nondestructive testing, including ultrasonic inspection. Level II is the intermediate qualification level for an inspection technique.
[7] MiniProf® is a portable precision contact measurement tool designed to measure cross sections of rail and wheel profiles, manufactured by Greenwood Engineering, headquartered in Brøndby, Denmark.

side faced south. For the north rail fragments, the field side faced north. The direction of the train prior to derailment (east) is noted in the figures.

The recovered rail piece 12N is highlighted in Figure 16 through Figure 21. The rail fragment measured 5 feet, 2 inches. Figure 20 shows the field side web markings of the rail piece, which indicated it was manufactured by Inland Steel in January 1925.[8] Both fracture faces exhibited rough surface textures with random surface orientations and little local plastic deformation. These features were consistent with overstress failure of rail exhibiting relatively low ductility. There were no macroscopic indications of subsurface damage on these fracture surfaces that would be consistent pre-existing damage leading to early fracture of the rail.

Of note on this rail piece was the presence of rail batter on the field side of the head (Figure 19). This batter was consistent with wheel-rail contact on the west rail face after fracture. Figure 21 shows repeating dimpled chatter marks on the gage side of the rail. These marks were consistent with repeated wheel flange impacts on the gage side of the rail head.

Figure 22 through Figure 27 highlight the 10N and 11N rail fragments. Piece 10N measured 2 feet in length, and piece 11N measured 1 foot, 5 inches (along the base). The east fracture face of 10N and the west fracture faces of 11N were consistent with having mated prior to fracture. The fractured head portion of 11N was not recovered on-scene. Similar to 12N, all the fracture surfaces exhibited features consistent with overstress failure and were absent macroscopic indications of pre-existing subsurface cracks.

Figure 24 shows some chipping on the base of 10N. This chipping was consistent with the location of a rail anchor, where the derailment forces pulled the base away from the anchor. Figure 25 shows gage side chatter and deformation on 10N. However, there were no visual indications of more severe damage consistent with extensive rolling contact fatigue or head wear (Figure 26 and Figure 27).

Figure 28 through Figure 32 highlight rail fragment 10S. This rail fragment measured 3 feet, 4 inches. As shown in Figure 28, Figure 29, and Figure 31, the west-facing fracture surface was a compound fracture that exhibited longitudinal and transverse orientations in the head, web, and base. The east-facing fracture surface, though, was more flat and transverse oriented, with features consistent with overstress fracture (Figure 30).

Of note on the 10S east-facing fracture was head batter. The batter was present on much of this fracture face, although it was generally angled facing the field side. The orientation of the angled batter was generally parallel to the deviation marks on the running surface of the head (upper portion of Figure 31). In addition, as shown in Figure 32, the gage side of the head exhibited features consistent with rolling contact fatigue. Head checking, flaking, and shelling were all present on this rail fragment. These features are described more in Section 3.2.2 of this report.

[8] The Inland Steel Company was a United States steel company active from 1893 – 1998. It was headquartered in the Chicago, IL Inland Steel Building. Its remaining assets are now a part of ArcelorMittal, a multinational corporation headquartered in Boulevard d'Avranches, Luxembourg.

Figure 33 and Figure 34 highlight two major features of rail piece 4S, which measured 9 feet, 4 inches. Figure 33 shows a sawtooth fracture in the web near the west-facing fracture surface. No head batter was observed on this fracture surface. The head portion was generally deformed outward or toward the field side, while the base was generally deformed toward the gage side. These features were consistent with a shear overstress fracture through the web, which would be consistent with derailment forces directed toward the south side of the track. The markings on the rail indicated it was manufactured in November of 1946 by U.S. Steel (Illinois Facility).[9]

This rail piece also exhibited heat tinting on the rail head running surface (Figure 34). This was consistent with the effects of the post-derailment fire, and was not located at a weld or other manufacturing feature.

3.2.2. Visual Observations after Sectioning

Four of the fracture surfaces for 4S, 10S, 10N, and 12N were sectioned from the rail fragments. Additional 1-inch thick cross sections were taken through these rail pieces adjacent the fracture surface sections. Height and width measurements of these cross sections were taken and are compiled in Table III.

The east-facing fracture surface of fragment 10N is shown in Figure 35 and Figure 36, before and after cleaning, respectively. Fragment 11N, which mated with 10N, consisted only of the base and part of the web (Figure 37). Pieces 10N and 11N exhibited features typically consistent with pre-existing fracture, such as discoloration and a general curved thumbnail shape. However, later examination using a scanning electron microscope (SEM) showed that the fracture features on these pieces were inconsistent with pre-existing or progressive failure modes (Section 3.3).

The fracture surface features in the web of the fracture surfaces of both pieces extended into the base. These fracture features were inconsistent with having originated in the head of the rail. Rather, the features suggest that this fracture initiated in the web, approximately 2.75 inches from the bottom of the base, on the gage side. There were no discernible visible material or mechanical defects noted on the gage side of the web.

Also of note on fragment 10N was a chip on the field side of the base. This fracture exhibited features consistent with overstress. The chip was consistent with the base of the rail fragment being moved while still anchored.

A cross section of the 10N fragment is shown in Figure 38. Figure 39 shows an overlay of a new 90-lb rail profile for qualitative reference. Figure 39 was consistent with the measured head loss values in Table III, showing approximately 0.2 inches of head loss for 10N.

[9] The United States Steel Corporation, more commonly known as U.S. Steel, is an American integrated steel producer headquartered in Pittsburgh, PA.

Figure 40 shows the edge of the discoloration difference on the 10N fracture surface, located at the web to base transition. This figure shows the location of SEM micrographs taken on this fracture surface, shown later in Figure 58 and Figure 60.

Figure 41 shows a closer view of the batter present on the gage side of the rail fragment. These features were consistent with repeated batter from the wheel flange(s) in contact with this portion of the rail.

Figure 42 and Figure 43 show the east-facing fracture surface of rail piece 12N, before and after cleaning, respectively. The cleaned fracture surface exhibited features that were consistent throughout. The gage side of the rail piece exhibited corrugated dimpling, consistent with repeated sliding contact with an adjacent wheel. The fracture surface features of fragment 12N were consistent with overstress.

Of note was the batter and deformation on the gage side corner of the head of 12N (see Figure 45 and Figure 46). The radial lines of the head fracture surface were consistent with fracture initiation in this region. A closer view in Figure 47 shows some local deformation on the gage side of this region. However, later examination using a SEM did not reveal features that would have been consistent with pre-existing damage, such as progressive cracking.

A cross section of the 12N fragment is shown in Figure 47. Figure 48 shows an overlay of a new 90-lb. rail profile for qualitative reference. Figure 48 was consistent with the measured head loss values in Table III: approximately 0.2 inches of head loss for 12N.

The sectioned west-facing fracture surface of piece 10S is shown in Figure 49. This fragment exhibited a fracture surface on the west-facing side of the rail consisting of transverse and vertical components (Figure 50). Head batter was also present on this fracture. This batter was consistent with the running direction of the train (towards the east). The undamaged fracture surfaces on this fragment were all consistent with overstress. There were no indications of pre-existing cracks on the batter-free portions of the fracture surface.

An angled deviation mark was present on the running surface of the head of 10S (see Figure 51). The measured angle of deviation was approximately 5° toward the field side of the rail. Similarly, on the 10N north rail fragment, a parallel deviation mark was present on the head running surface (see Figure 52). The measured angle of deviation was approximately 6° toward the gage side of fragment 10N.

Sections of the 10S piece show the head checking and later shelling damage on the gage side of the 10S piece (Figure 53). A pronounced shell near a battered portion of the gage side is shown in Figure 54. This region was cross-sectioned and examined using optical metallography, as detailed in Section 3.4.

A cross section of the 10S fragment is shown in Figure 55. Figure 56 shows an overlay of a new 90-lb. rail profile for qualitative reference. Figure 56 was consistent with the measured head loss values in Table III, showing less than a 0.125 inches head loss for 10S.

A cross section of the 4S fragment is shown in Figure 57 with an overlay of a new 90-lb. rail profile for qualitative reference. As recorded in Table III, this piece exhibited less head loss than the other cross-sectioned pieces, consistent with the rail piece being manufactured more recently. This head loss was less the other cross-sectioned pieces of north rail, but was also fabricated more recently by a different manufacturer.

3.3 Scanning Electron Microscopy

Some of the fracture surfaces from the rail pieces were inspected using a scanning electron microscope. Two regions of the fracture surface of 10N were examined, as shown in Figure 40. A typical area of the fracture surface from the darker-colored portion of 10N is illustrated in Figure 58. This portion of the fracture surface exhibited cleavage facets, consistent with overstress fracture of a less ductile metal alloy.[10] At higher magnifications, the cleavage facets exhibited observable rounding (Figure 59). This rounding was consistent with surface oxidation, typical of fractured steels exposed to air, particularly at elevated temperatures.

A typical area of the shinier portion of the 10N fracture surface (outside the darker region) is illustrated in Figure 60. This region exhibited cleavage fracture features, consistent with SEM examination of the darker portion of the 10N fracture surface. A closer view of the features in Figure 60 revealed a banded arrangement (see Figure 61). Closer examination of these features found them to be consistent with lamellae in the pearlitic microstructure, typical of carbon steel (see Figure 62). No features consistent with other fracture modes were observed. This chemical composition of the 10N fracture surface was inspected using energy dispersive x-ray spectroscopy (EDS). The composition was found to be consistent with a carbon steel.

The area highlighted on the gage corner of 12N, shown in Figure 46, was examined using a SEM. This region revealed cleavage features consistent with those in Figure 58 through Figure 62. No features consistent with other fracture modes or pre-existing cracking were observed in the gage corner of the 12N fracture surface.

3.4 Optical Metallography

The head of the 10S cross section was ground and polished to 0.3 μm. The gage side of the polished cross section is shown in Figure 63. This cross section illustrated a sub-surface shell crack. The shell crack was present at a depth of 0.150 inches below the running surface, and extended 0.449 inches from the gage side into the head. Other smaller cracks were present on the gage side.

[10] Cleavage fracture is a fracture of crystalline material along specific low-index crystallographic planes, resulting in reflective facets.

Figure 64 shows the same cross section, after etching with 2% Nital. The overall grain size was visibly smaller near the running surface, where the subsurface cracks were also present. Figure 66 shows a typical area of the rail microstructure, away from the running surface. The microstructure consisted of pearlite and ferrite, consistent with a typical microstructure for a near-eutectoid carbon steel.

Figure 67 shows a region closer to the running surface of the head. The microstructure, while still comprised of pearlite, also exhibited a compressed and flattened grain structure. This grain texture was generally parallel to the internal shell cracks present in the gage corner of the head cross section. The right side of the figure exhibited some white-colored material. This was consistent with untempered martensite, which would be consistent with a portion of the steel experiencing temperatures above 770°C (1418 °F), and then rapidly cooled. It should be noted the dark blue regions adjacent to the shell cracks in Figure 67 were etch stain artifacts from etchant flowing into the openings.

3.5 Hardness Testing

Four of the examined rail head cross sections were Rockwell hardness tested per ASTM E18.[11] The hardness indents were performed at locations prescribed in *AREA Manual for Railway Engineering*.[12] This standard prescribes three measurements approximately at mid-head height, and two additional measurements 0.375 inches each from the field and gage faces of the cross section. A diagram showing the locations for the seven prescribed hardness indents is illustrated in Figure 68.

The results of the hardness testing on the cross-sectioned rail heads for pieces 4S, 10S, 10N, and 12N are illustrated in Figure 69. In addition, Figure 65 shows the hardness measurements conducted on the polished and etched cross section from piece 10S. This figure shows the hardness values (from gage side to field side) were 21 HRC, 18 HRC, and 22 HRC. At the two locations near the lower field and gage corners, the hardness values were 18 HRC and 21 HRC at the gage and field sides, respectively.

Overall, the hardness data were consistent with those typical for a softer carbon steel. The average hardness values for each rail head cross section tested were: 23 HRC for piece 4S, 20 HRC for piece 10S, 20 HRC for piece 10N, and 21 HRC for piece 12N. When converted to Brinell hardness values per ASTM E140, these data were 243 HB, 226 HB, 226 HB, and 231 HB, respectively.[13]

---

[11] ASTM E18 – *Standard Test Methods for Rockwell Hardness and Rockwell Superficial Hardness of Metallic Materials*. ASTM International, West Conshohocken, PA.
[12] American Railway Engineering Association, *Manual for Railway Engineering, Chapter 4, Part 2: Specification for Steel Rails* (1998), p. 4-2-8
[13] ASTM E140 – *Standard Hardness Conversion Tables for Metals Relationship Among Brinell Hardness, Vickers Hardness, Rockwell Hardness, Superficial Hardness, Knoop Hardness, and Scleroscope Hardness*. ASTM International, West Conshohocken, PA.

The minimum required tensile strength was 85000 psi for rail, according to a 1969 specification by AREA.[14] The above hardness data satisfy this requirement for rail with carbon contents above 0.45 weight percent (wt. %). The 1998 standard for rail does not have requirements for 90-lb. rail. This standard requires minimum hardness for “standard rail” of 300 HB at a depth of 3/8 inches depth on points 1, 2, or 3 in Figure 68.[12]

3.6 External Testing Results

The chemical compositions of specimens from rail heads for 4S, 10S, and 10N were inspected by Lehigh Laboratories.[15] The specimens were inspected using inductive couple plasma (ICP) optical emission spectroscopy (OES), with additional analysis for carbon and nitrogen as well as vacuum hot extraction for hydrogen per ASTM E146-83.[16] The data are compiled in Table IV.

The chemical compositions inspected generally met the requirements for the 1979 AREA requirements for 90-lb rail. The exception was the manganese (Mn) content for the specimen from 10S, which was less than the minimum requirement of 0.70 weight %.

Erik Mueller
Materials Research Engineer

[14] American Railway Engineering Association, *Manual for Railway Engineering, Chapter 4, Part 2: Specification for Steel Rails* (1979), p. 4-2-9
[15] Lehigh Testing Laboratories, Inc. is an independent materials testing laboratory located in New Castle, DE.
[16] ASTM E146-83 – *Methods of Chemical Analysis of Zirconium and Zirconium Alloys (Silicon, Hydrogen, and Copper)*. ASTM International, West Conshohocken, PA. This standard has been withdrawn without replacement.

Table I – Inventory of Recovered North Rail from Accident Site

Piece #	Length (ft.)	Cumulative Length from West (ft.)	PW1 Length (ft.)	PW2 Length (ft.)	Distance from last PW (ft.)	**West end description**	**East end description**	**Notes on Piece**
0N	30.6	30.6	N/A	N/A		Saw cut	Torch	
1N	43.3	73.9	7.2	42.0	34.8	Torch cut	At HC	HC
2N	37.5	111.4	34.1		35.4	At HC	Head and base heavy gage side contact	HC
3N	9.3	120.6				Head and base heavy gage side contact	At HC	HC
4N	23.3	143.9	23.3		35.9	At HC	At PW	HC, Wheel leaving mark
5N	25.2	169.0				At PW	Rub in web	
6N	10.1	179.1	10.1		35.3	Minimal RB, rub at upper web, wheel marks	At PW	HC
7N	6.8	185.9				At PW		
Missing		185.9						
8N	3.6	189.5					Heavy contact gage side of head	
9N	13.9	203.4	11.5		21.8	Heavy contact gage side of head		
10N	2.0	205.4					Preexisting split web?	
11N (base)	1.4	206.8				Preexisting split web?	Head/web separation	
12N	5.2	212.0				Heavy RB, rub on gage side of head		
Missing		212.0						
13N (base)	2.3	214.3						
14N	1.6	215.9					At HC	HC, flakes
15N(A) (head)	3.5	219.4				At HC		HC, flakes
15N(B) (base)		219.4						

16N (head)	1.3	220.6						HC
Missing	3.8	224.4						
17N	3.4	227.8					At HC	HC
18N	15.8	243.6				At HC	Fire deposits	HC
19N	10.4	254.0	7.7		50.3	Fire deposits	At HC	HC
20N	32.0	286.0	32.0		34.8	At HC, Heavy RB	At PW	HC, flakes
21N	12.8	298.8				At PW	At HC	HC
22N	3.5	302.3				At HC	From HC	HC
23N	32.3	334.6	19.9		36.2	From HC		HC
24N	21.3	355.9					Recovery break	
25N	76.4	432.3	2.4	66.3	36.2	Recovery break	Torch	
Total	432.3							
Survey	432.3							
Missing total	3.8							

Table II – Inventory of Recovered South Rail from Accident Site

Piece #	Length (ft.)	Cumulative Length from West (ft.)	PW1 Length (ft.)	PW2 Length (ft.)	Distance from last PW (ft.)	West end description	East end description	Notes on Pieces
0S	30.6	30.6	N/A	N/A		Saw cut	Torch	
1S	66.8	97.3	11.1	48.0	36.9	Torch	Torch	
2S	10.2	107.5	0.0			Torch		HC, flakes
3S	38.5	146.0	6.7		37.4	Minimal RB	LB, Heavy flanging	
Missing	2.7	148.7	0.0					
4S	9.3	158.0	0.0			Split web, RB on gage side face of head		
5S (head)	2.4	160.4	0.0					
Missing		160.4	0.0					
6S	31.7	192.1	26.5		72.7	RB, flange mark in web		
7S	26.2	218.2	0.0				LB	
8S (base)	1.9	220.2	0.0					
9S	9.6	229.7	2.5		35.8	Heavy RB	Flange mark riding up	HC
Missing	12.5	242.2	0.0					
10S	3.3	245.6	0.0			Heavy RB		HC
11S	46.7	292.2	15.3		38.2		From HC	HC, flakes
12S	8.2	300.4	3.6		35.0	From HC	LB	
13S	5.5	305.9	0.0			Minimal RB		HC, flakes
14S	36.8	342.7	26.3		36.4		From HC	HC, Flakes
15S	89.6	432.3	24.7	48.0	35.2	From HC		
Total	432.3							
Missing total	15.2							

Table III – Rail head height and width measurements of the cross sections from each rail fragment.

Measurement Location	Rail Height (in) East Fracture	Vertical Head Loss (in)	Rail Height (in) West Fracture	Vertical Head Loss (in)
10N	5.414	0.211	5.414	0.211
12N	5.401	0.224	5.423	0.202
14N	5.434	0.191	5.432	0.193
17N	5.410	0.215	5.490	0.135
3S	5.602	0.023	Torch Cut	N/A
4S	5.560	0.065	Torn Web	N/A
6S	Torch Cut	N/A	5.536	0.089
10S	5.539	0.086	5.501	0.124

Table IV – Results of the chemical analysis of the three rail specimens performed using ICP-OES at Lehigh Testing Laboratories. The table shows the results of the chemical composition, in weight %, of each element (except H, which was reported in ppm). The elements in bold had minimum and/or maximum requirements in the AREA specification for rail.[12] The balance of the material weight percent was iron (Fe).

Element	4S (Weight %)	10N (Weight %)	10S (Weight %)
Carbon (C)	0.786	0.710	0.738
Sulfur (S)	0.028	0.028	0.027
Silicon (Si)	0.142	0.191	0.200
Phosphorus (P)	0.013	0.026	0.020
Manganese (Mn)	0.740	0.756	0.648
Nickel (Ni)	0.039	0.021	0.010
Chromium (Cr)	0.052	0.013	0.022
Molybdenum (Mo)	0.012	0.006	0.005
Copper (Cu)	0.068	0.094	0.012
Tin (Sn)	0.018	0.018	0.012
Aluminum (Al)	0.003	0.003	0.004
Titanium (Ti)	Not reported	0.003	0.002
Cobalt (Co)	0.005	0.007	0.004
Tungsten (W)	0.016	0.016	0.014
Zirconium (Zr)	0.003	0.003	0.003
Zinc (Zn)	0.005	0.004	0.004
Nitrogen (N)*	<0.01	<0.01	<0.01
Hydrogen (H)**	3.7 ppm	2.7 ppm	3.3 ppm

*Tested using a LECO nitrogen analyzer
**Tested using vacuum hot extract; reported in parts per million (ppm).

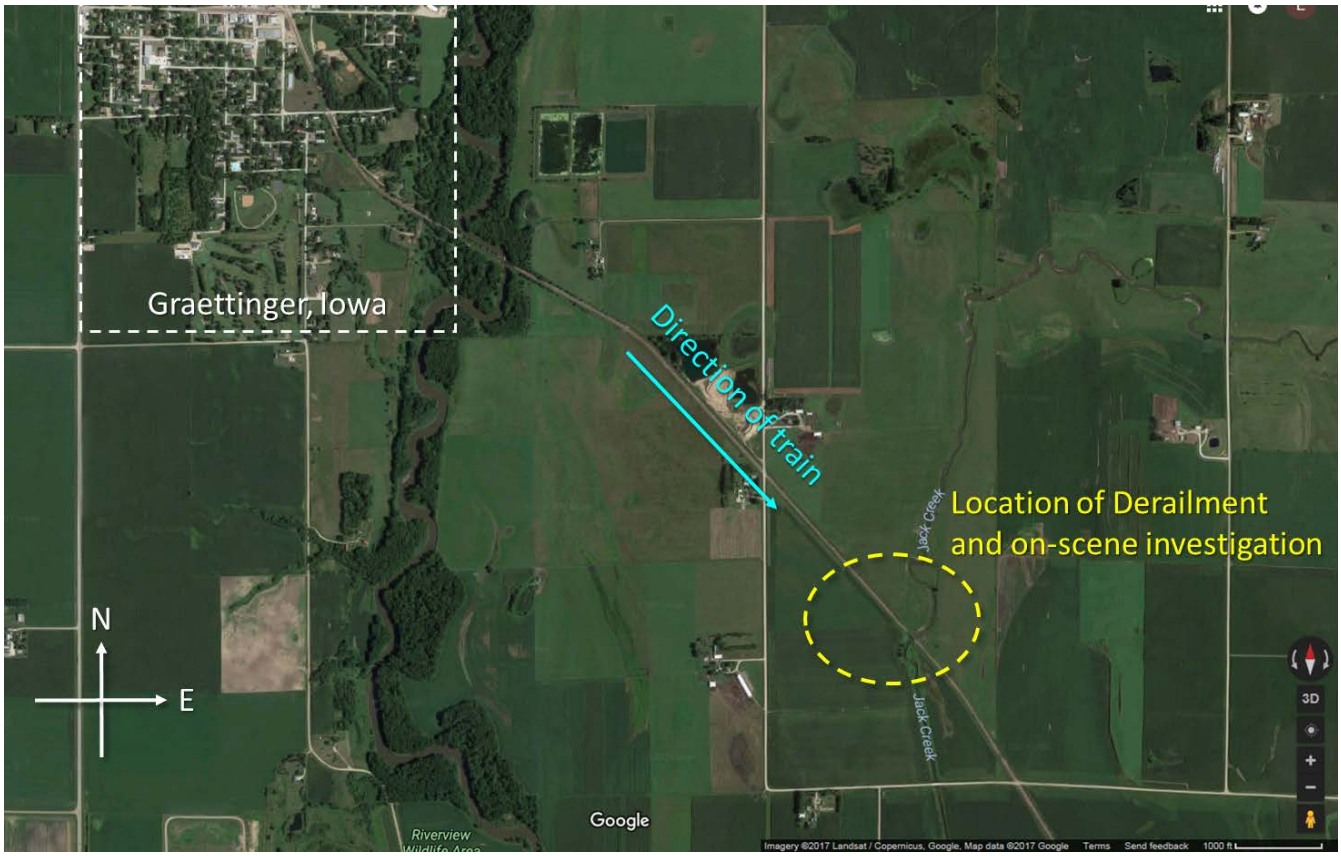

Figure 1 – Location of the derailment, relative to Graettinger, IA.

Figure 2 – Closer view of the derailment location, showing the north and south rail with the direction of train travel.

Figure 3 – A view of the rail reconstruction, facing toward the direction the train traveled (east).

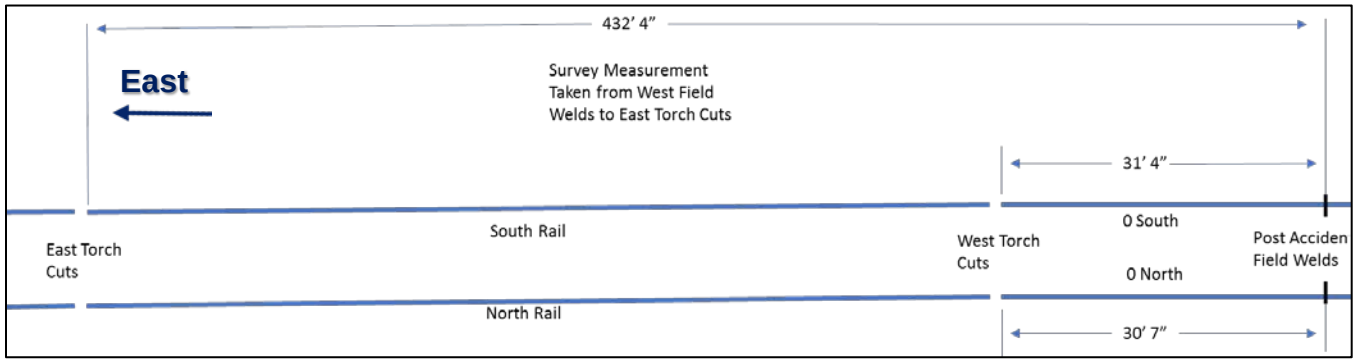

Figure 4 – Schematic showing the general layout of the track survey measurements of the derailment site. The train direction is toward the left in the figure.

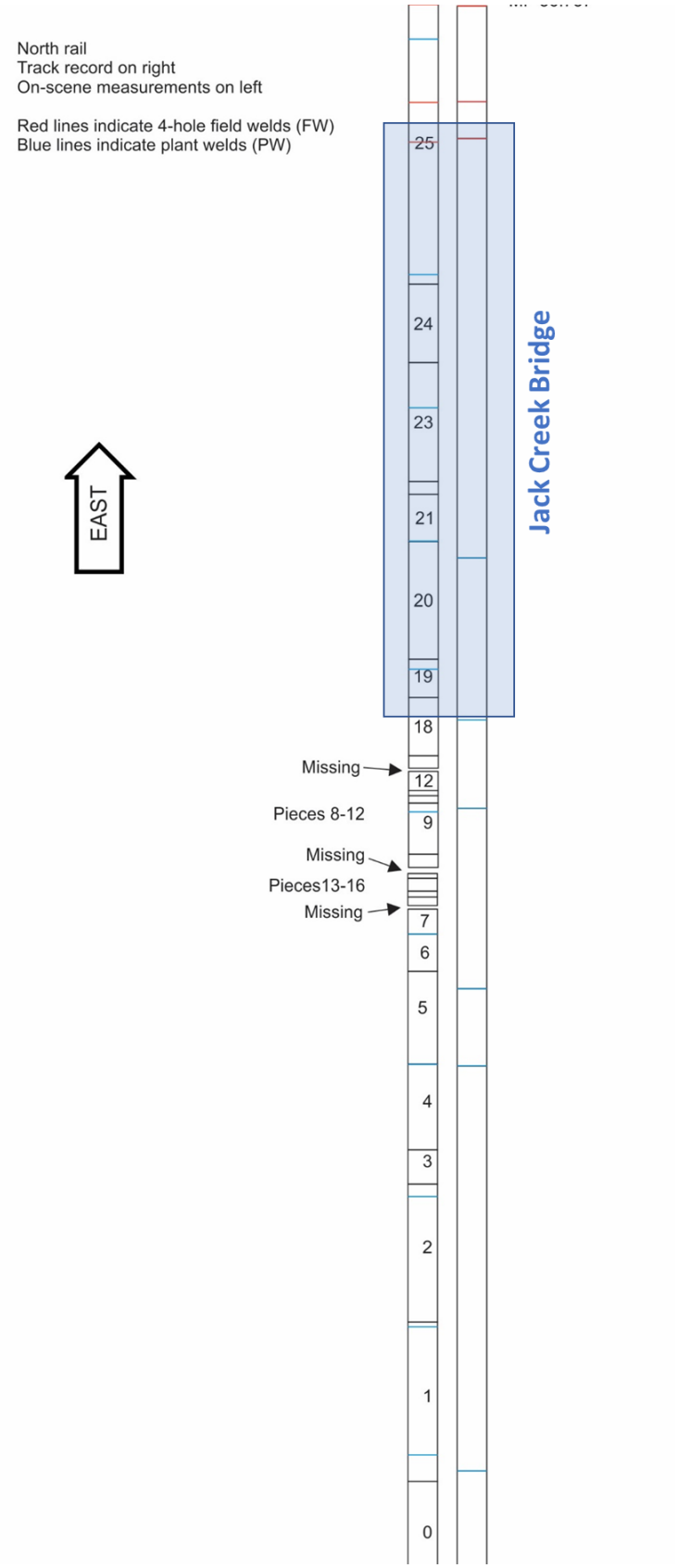

Figure 5 – Schematic representation of the collected north rail, shown in general order as reconstructed.

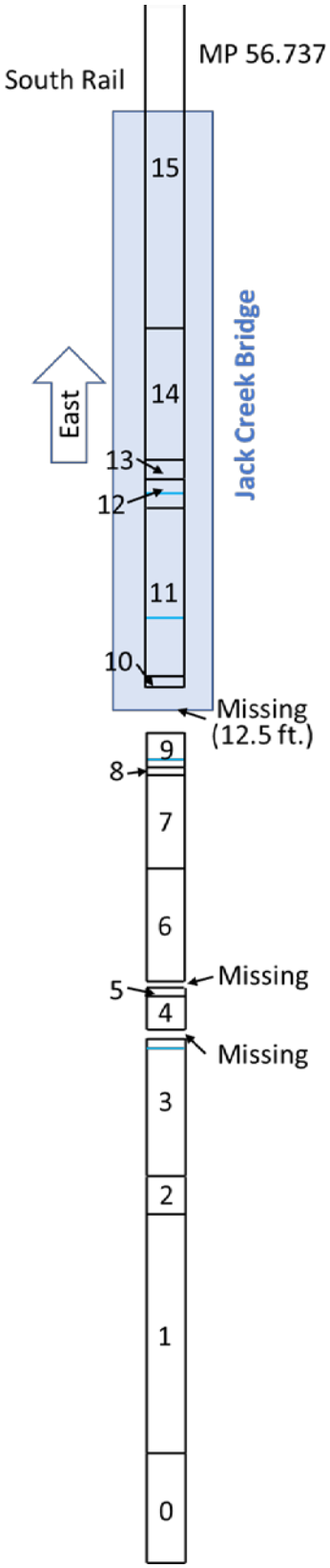

Figure 6 – Schematic representation of the collected south rail, shown in general order as reconstructed.

Figure 7 – The west-facing fracture surface of 20N, showing heavy rail batter, head checking, and flaking.

Figure 8 – Closer view of rolling contact fatigue on the gage side of 14N rail section.

Figure 9 – Rail piece 4S located where the plug rail and weld was located.

Figure 10 – From right to left, pieces 14N through 16N recovered on scene.

Figure 11 – The east-facing fracture surface of 18N, showing orange-colored residue on the running surface and fracture surface.

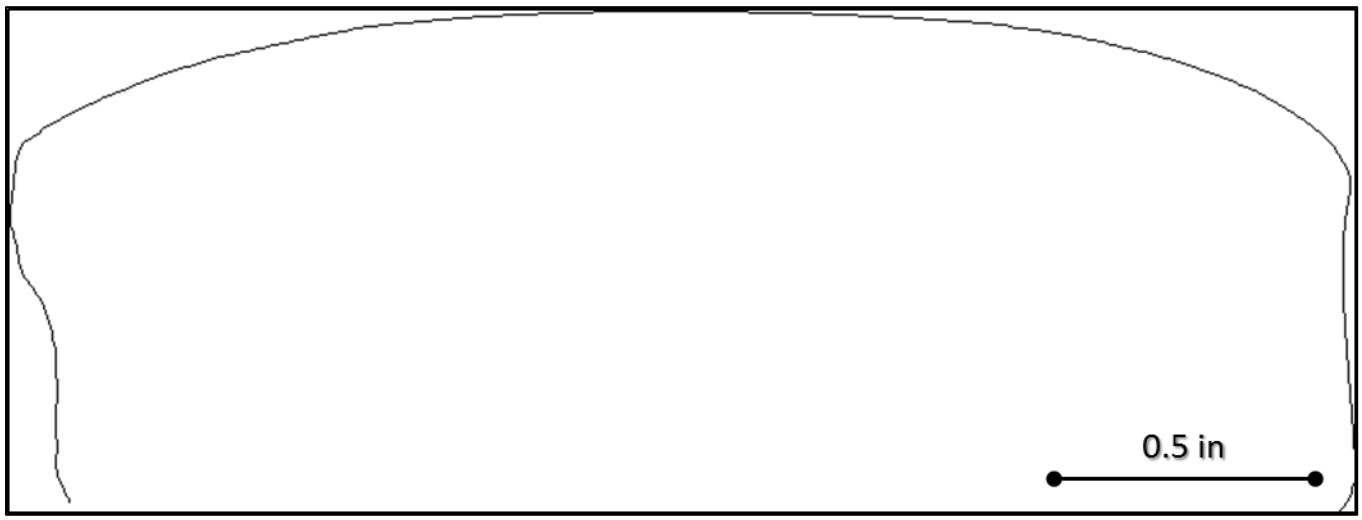

Figure 12 – The Miniprof profile of the 10N rail head (gage side faces left).

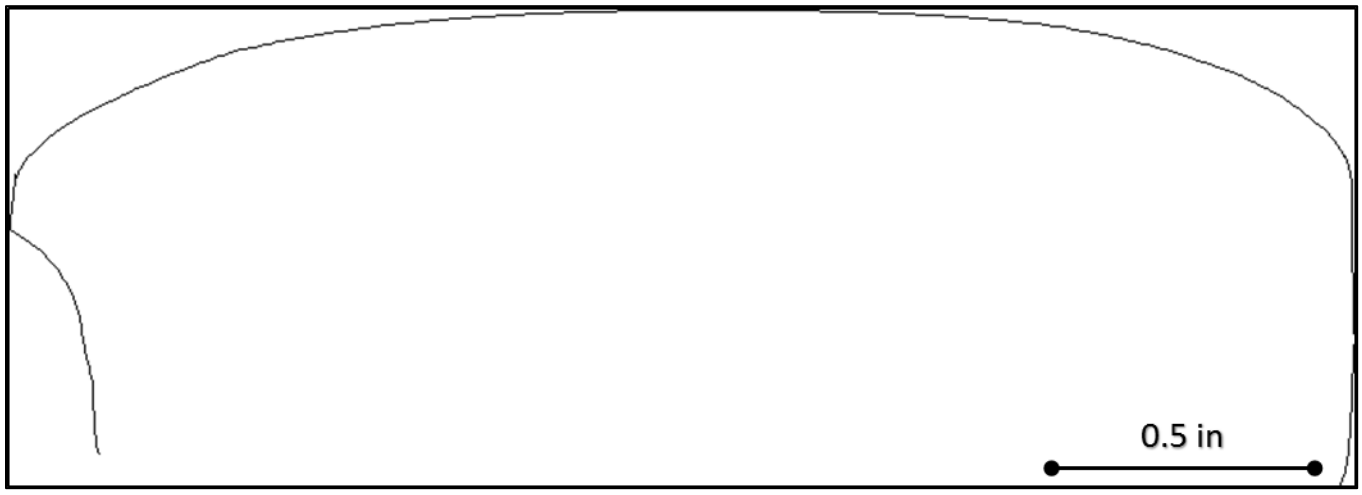

Figure 13 – The Miniprof profile of the 12N rail head (gage side faces left).

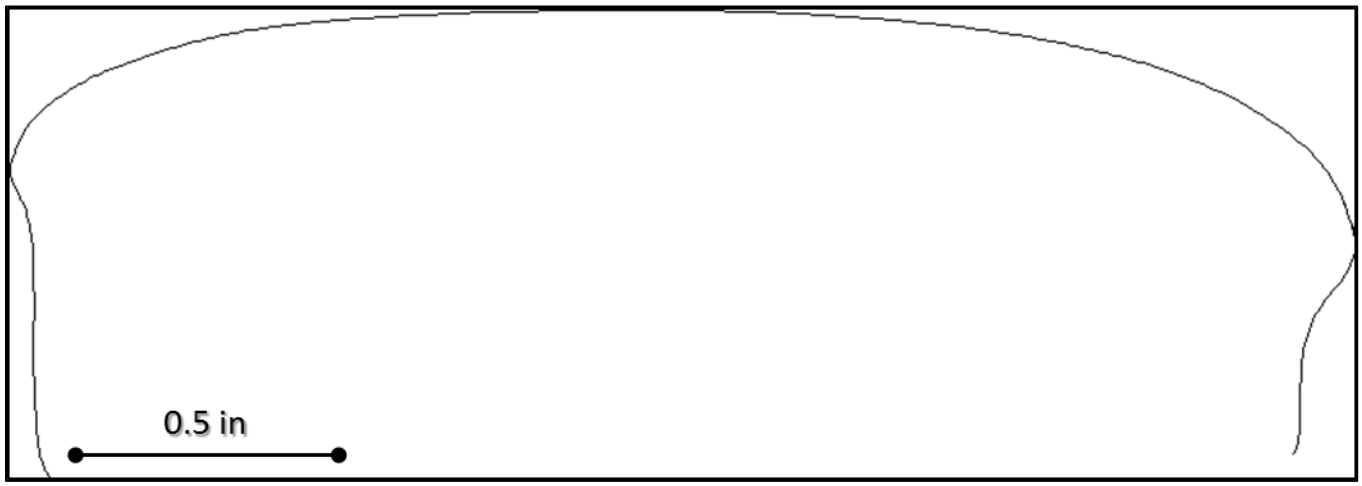

Figure 14 – The Miniprof profile of the 14N rail head (gage side faces right).

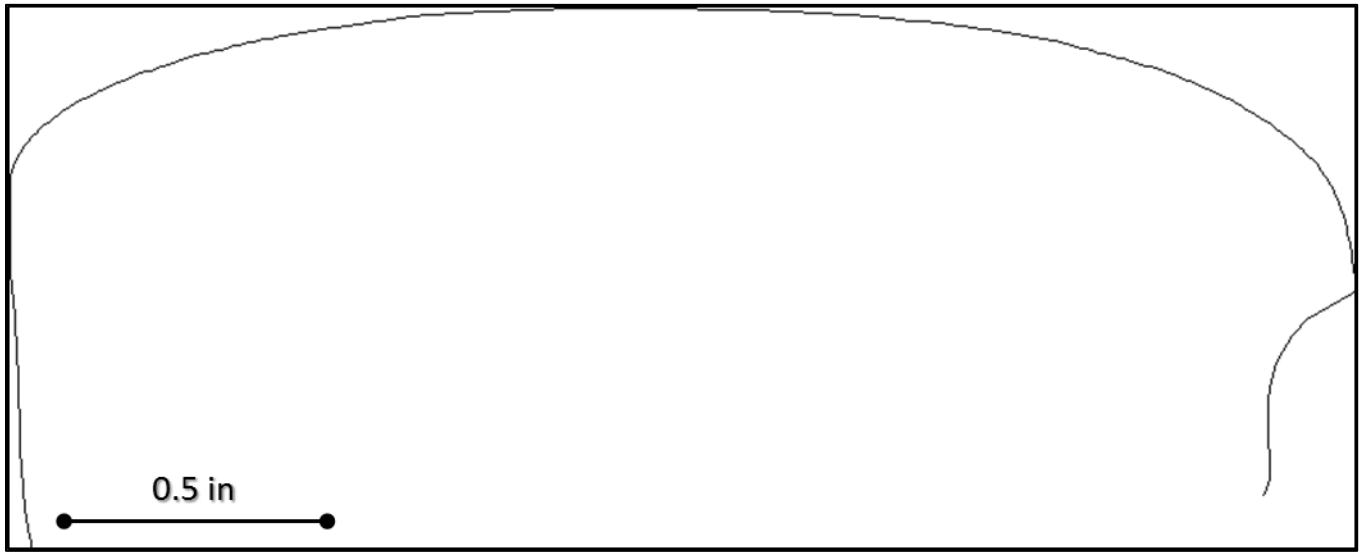

Figure 15 – The Miniprof profile of the 10S rail head (gage side faces right).

Figure 16 – The field side of the piece of north rail labeled 12N, as received.

Figure 17 – The gage side of the piece of north rail labeled 12N, as received. East is to the right.

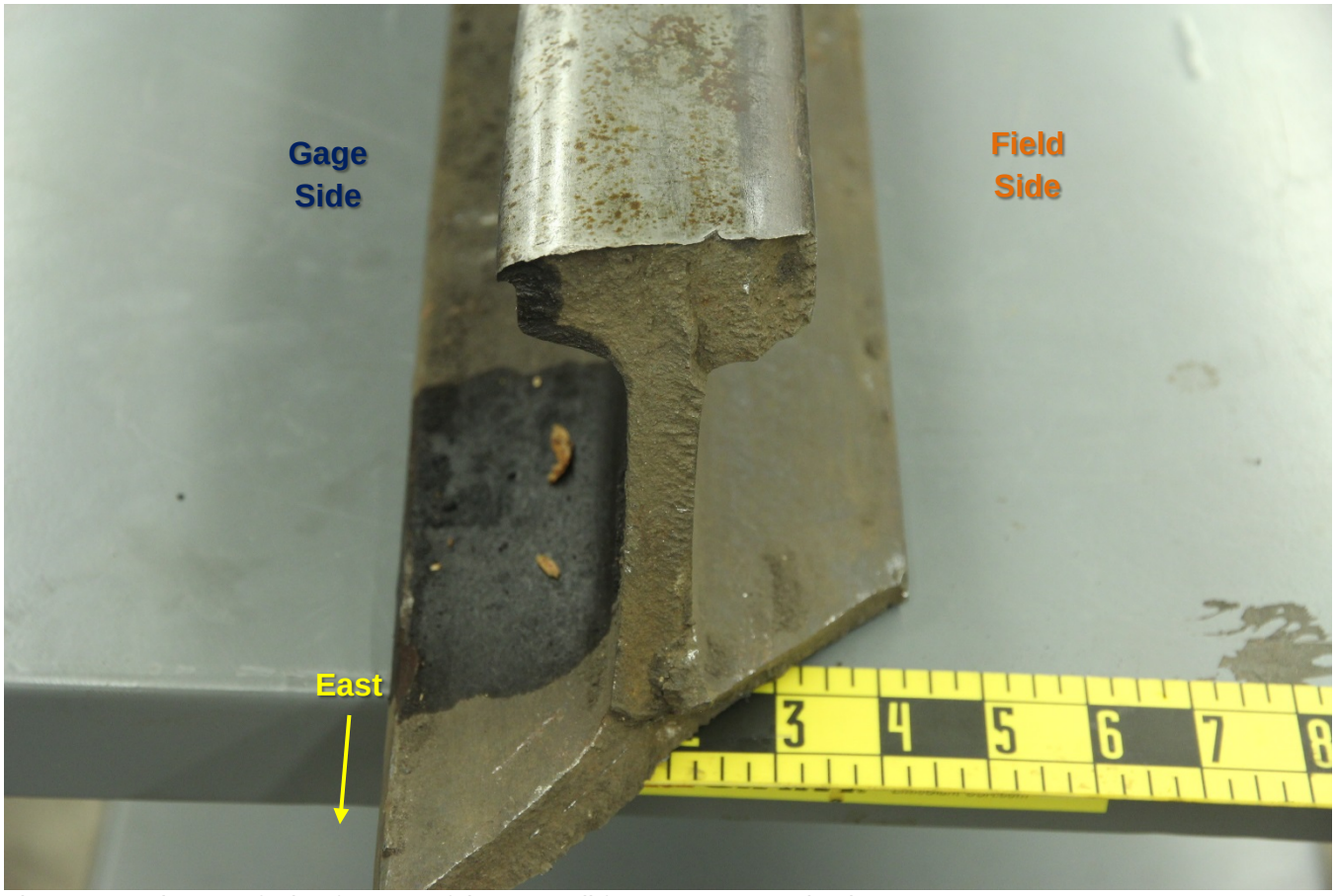

Figure 18 – The east-facing fracture of the 12N rail fragment, as received.

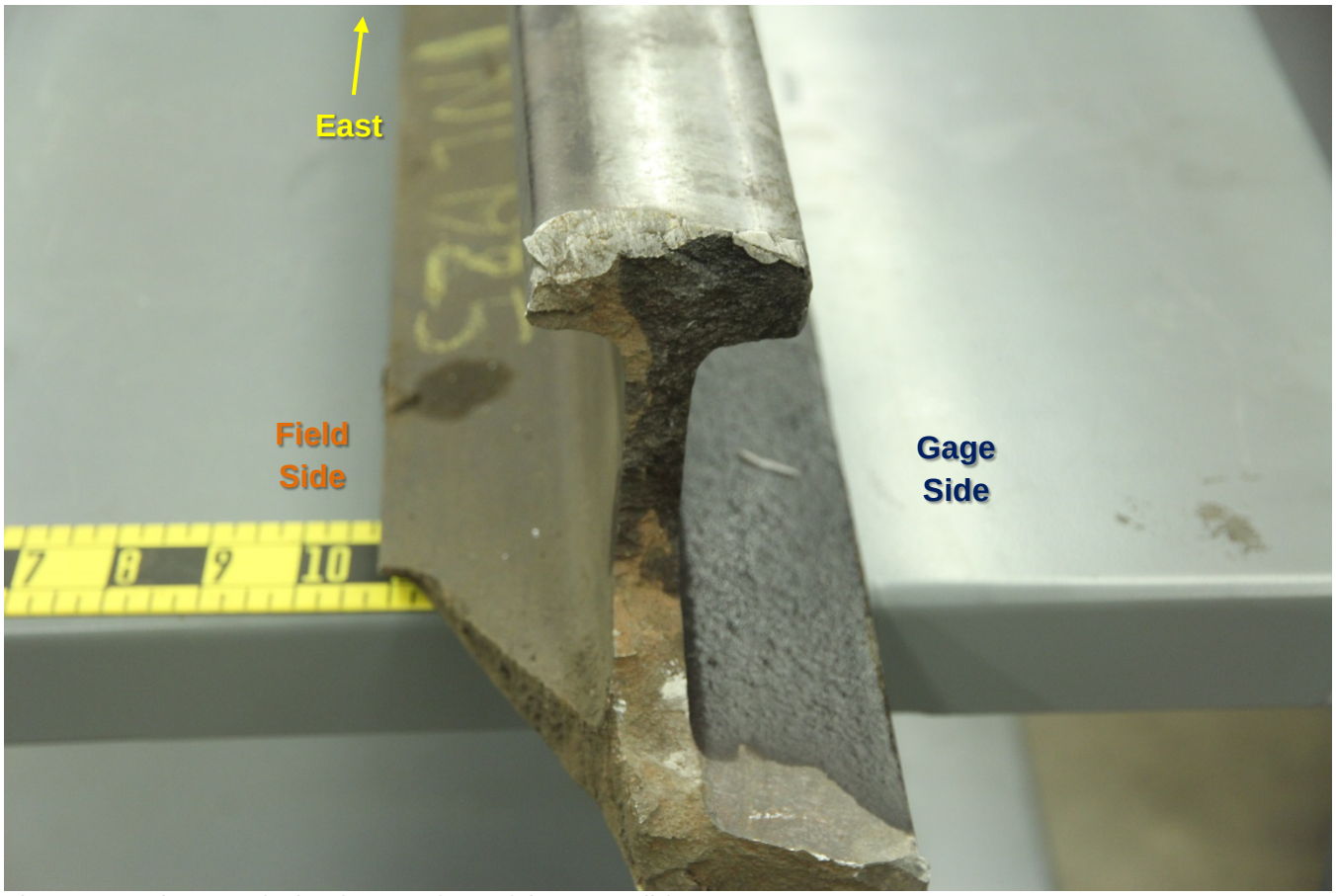

Figure 19 – The west-facing fracture face of the 12N rail fragment.

Figure 20 – Markings on the field side web of 12N rail fragment, indicating company and date of manufacture.

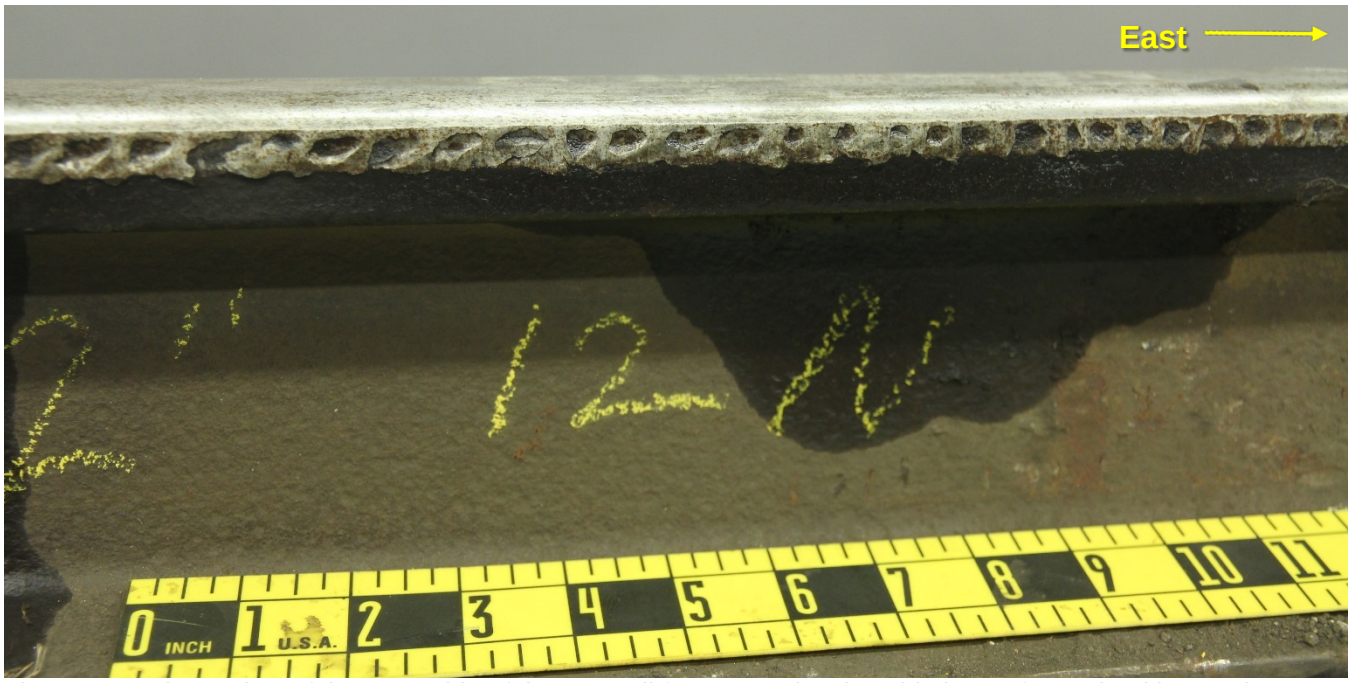

Figure 21 – Closer view of the gage side of the 12N rail fragment, showing side batter from wheel interaction. East is to the right.

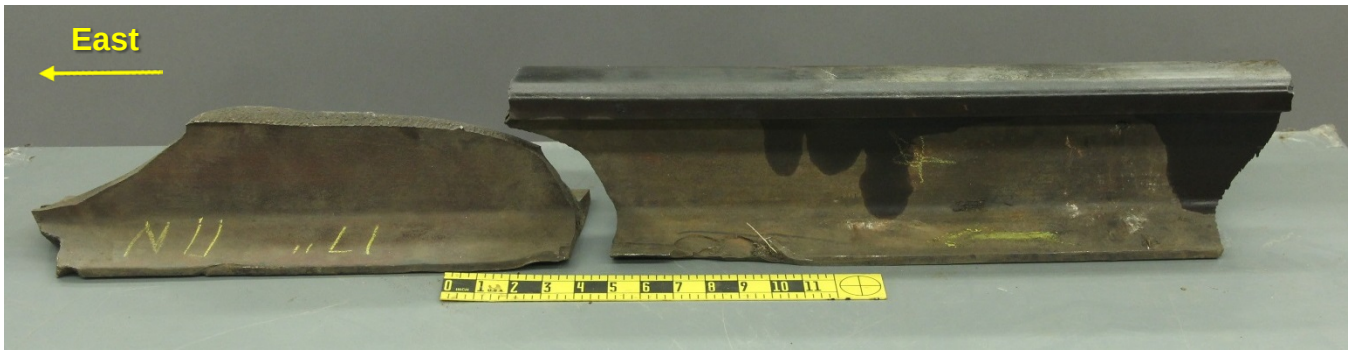

Figure 22 – The field side of the 11N and 10N fragments of north rail, as received. The east side is to the left.

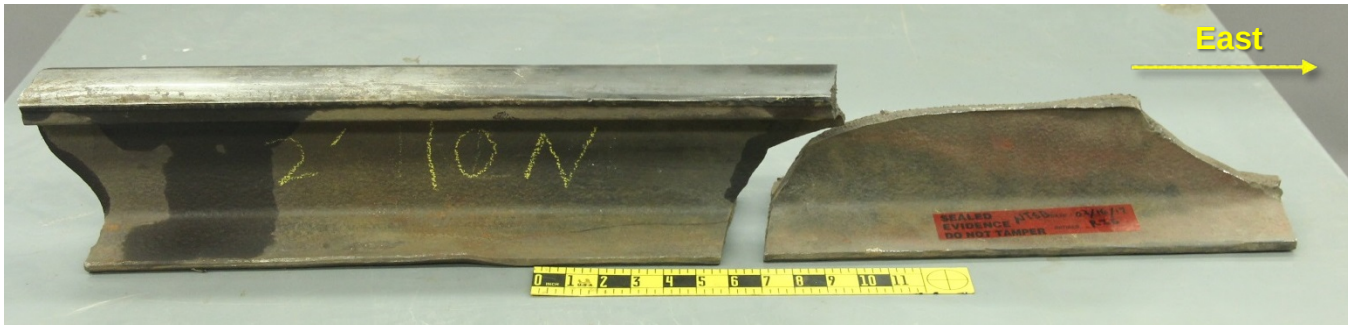

Figure 23 – The gage side of the 10N and 11N fragments of north rail, as received. The east side is to the right.

Figure 24 – Chipped piece of the field side base the 10N rail fragment.

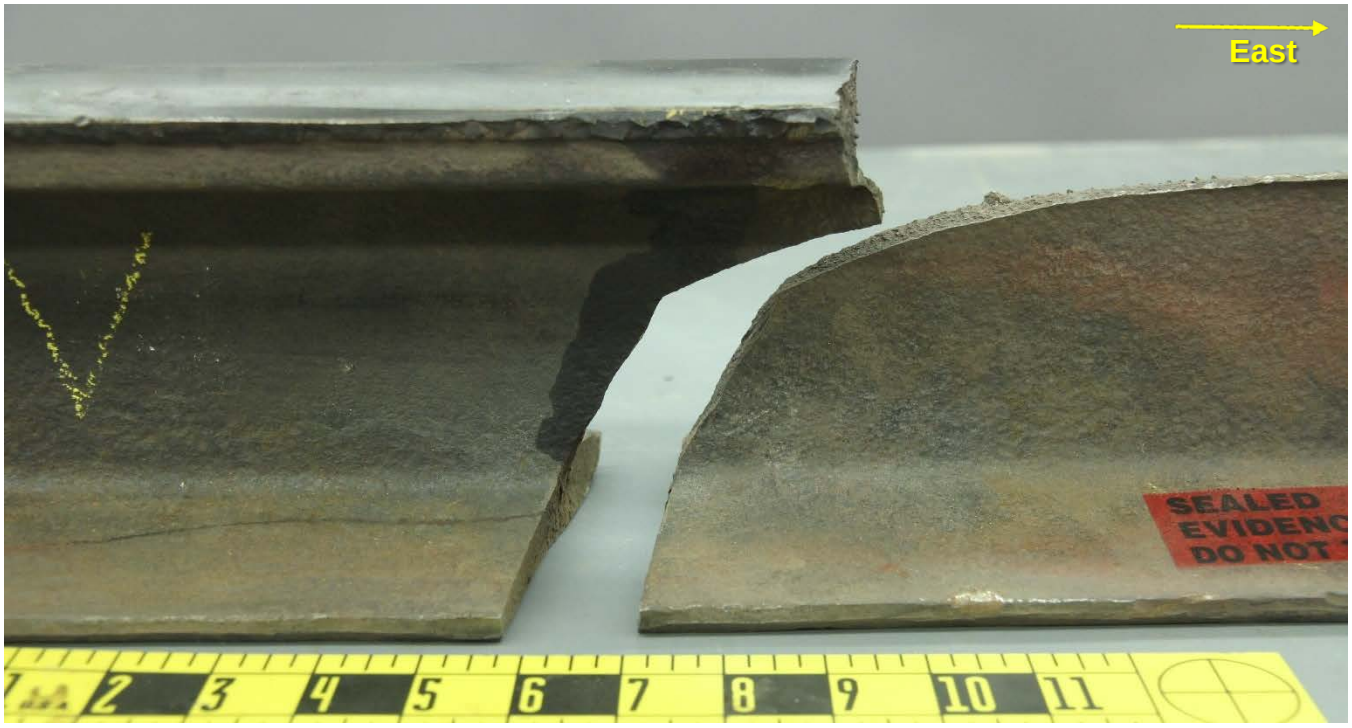

Figure 25 – Closer view of the mating fractures between the 10N and 11N fragments, from the gage side.

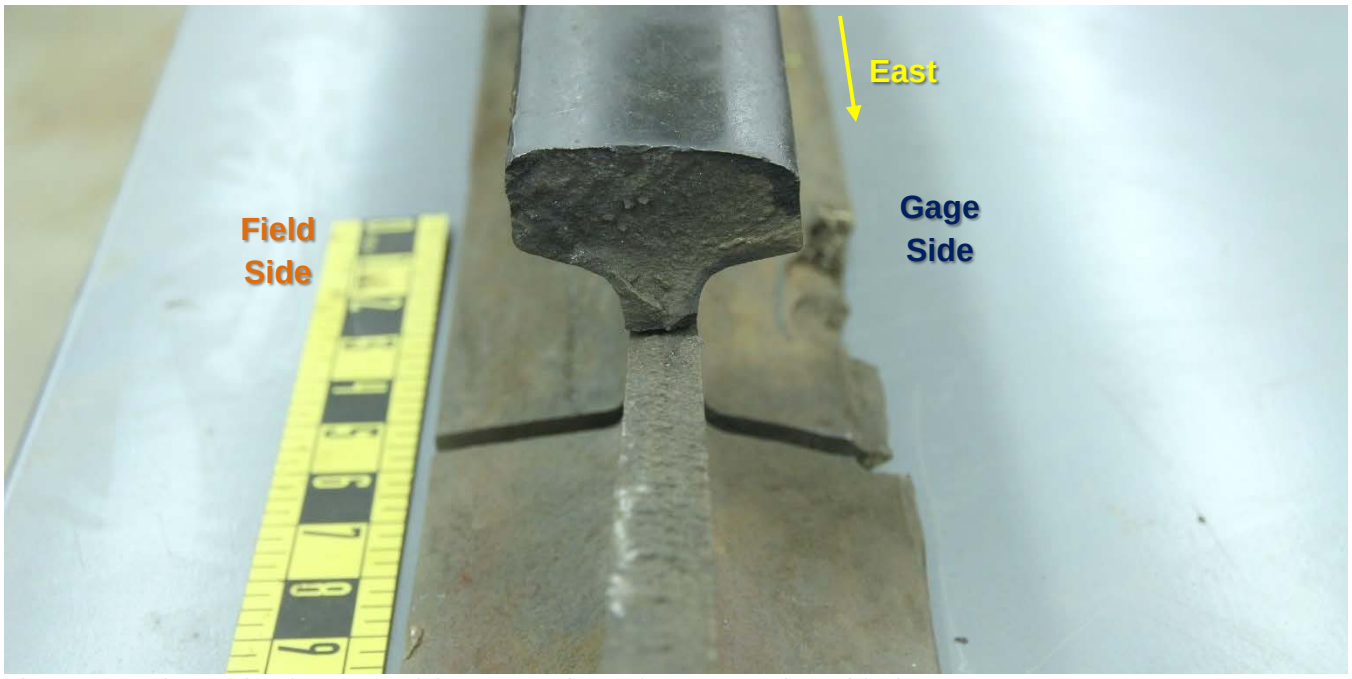

Figure 26 – The mating fractures of the 10N and 11N fragments, viewed facing west.

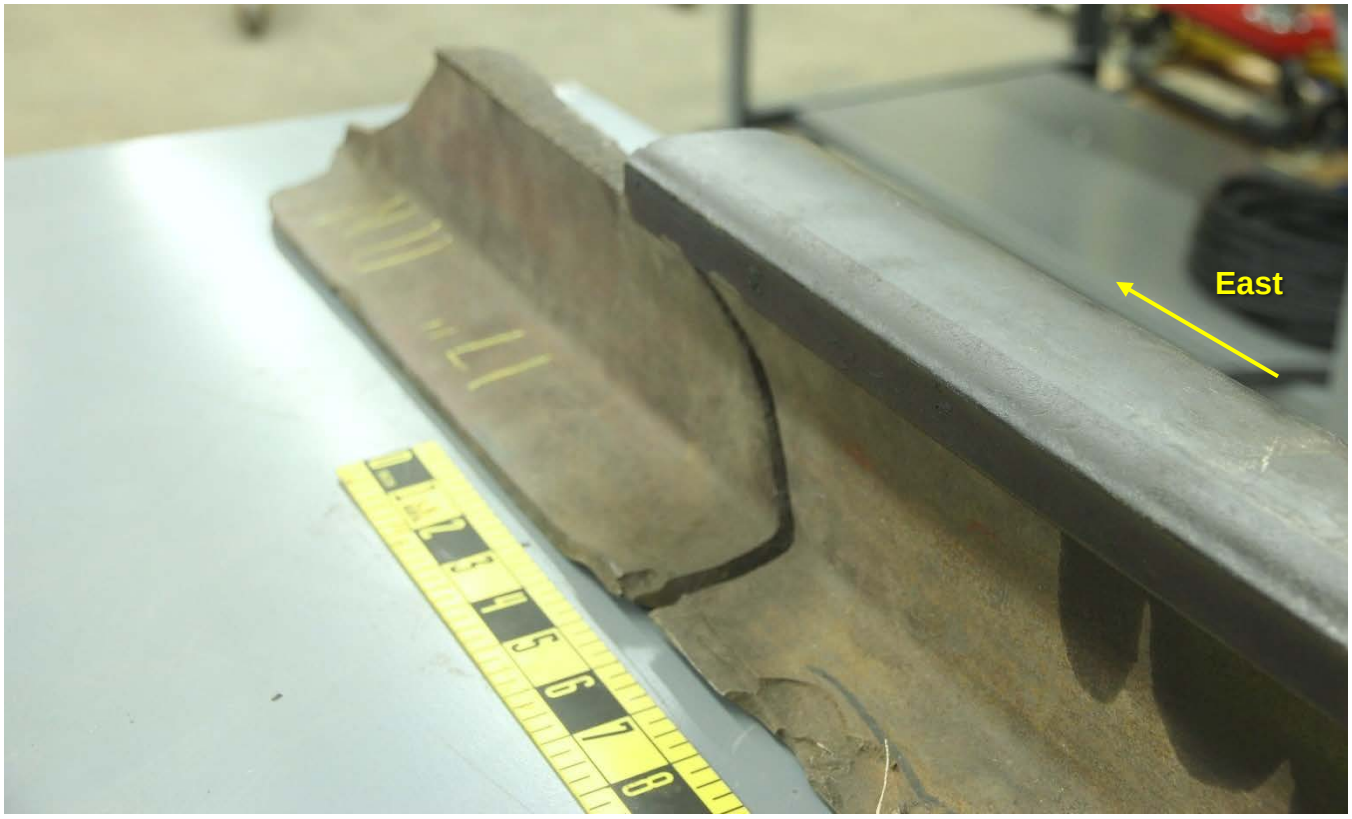

Figure 27 – The mating fracture surfaces of the 11N and 10N fragments, viewed from the field side.

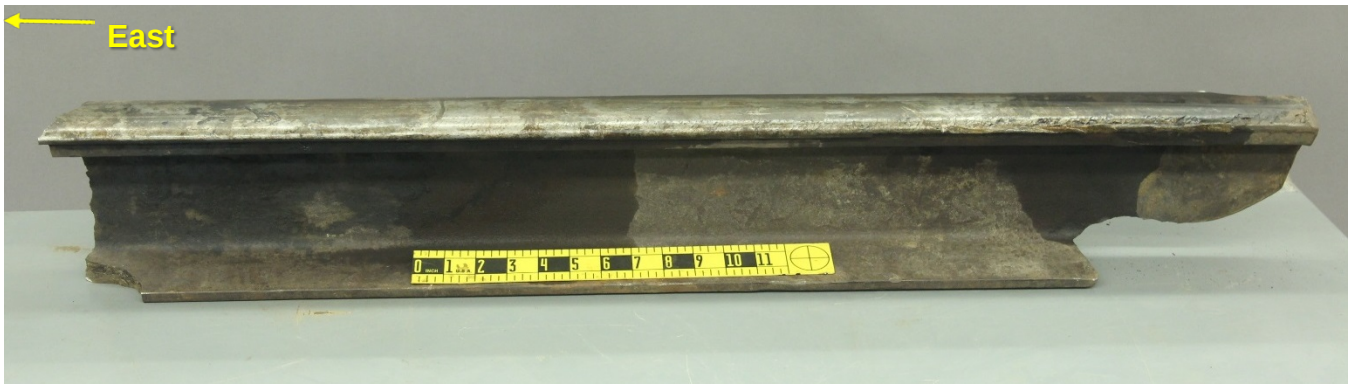

Figure 28 – The gage side of the 10S rail fragment from the south rail, as received.

Figure 29 – The field side of the 10S rail fragment, as received. The east direction is to the right.

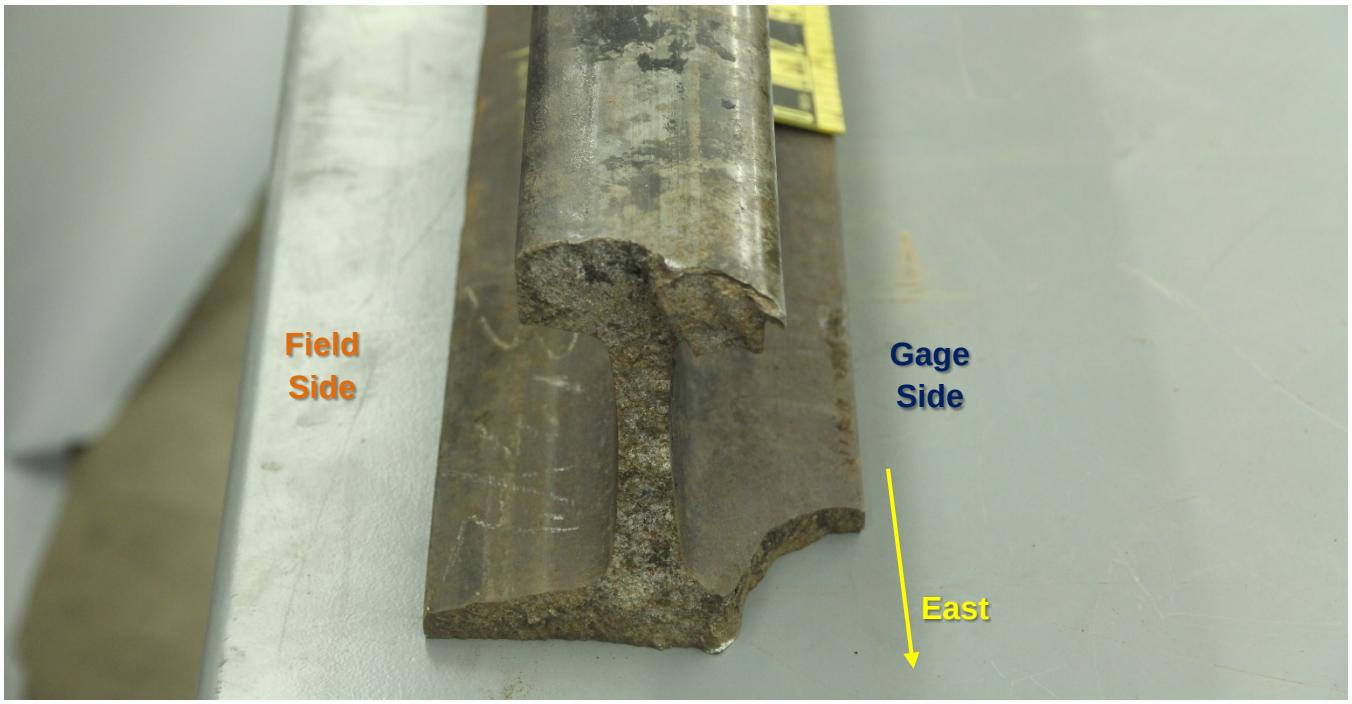

Figure 30 – The east-facing fracture surface of the 10S rail fragment.

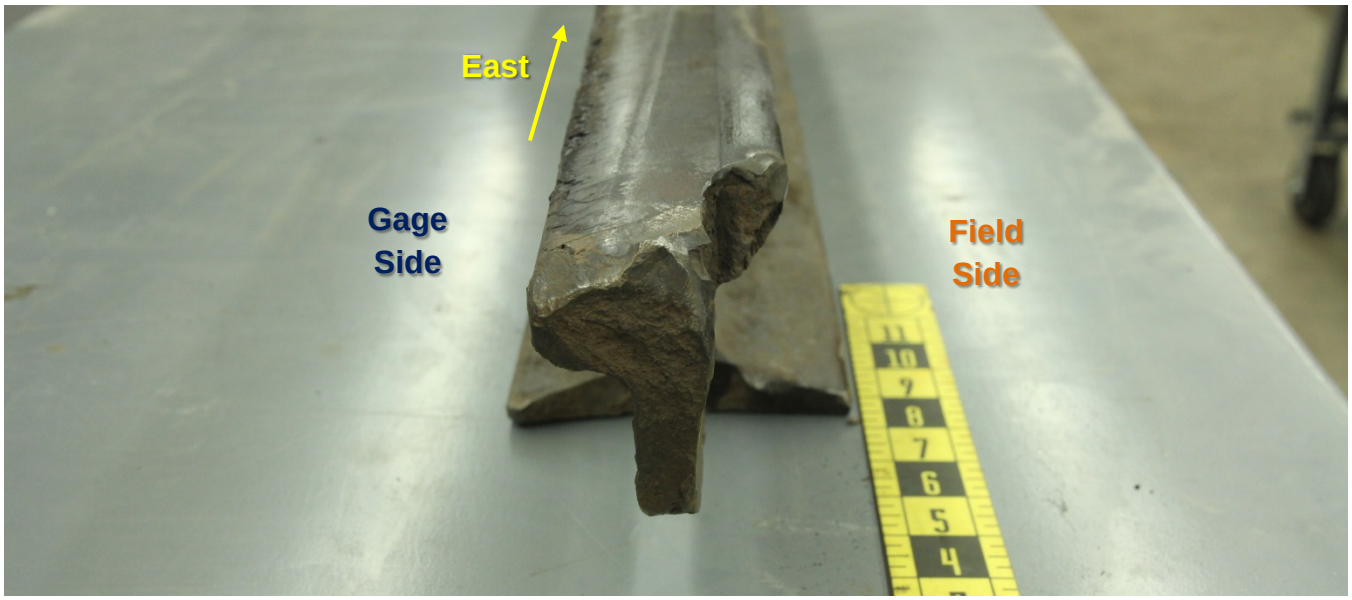

Figure 31 – The west-facing fracture surface of the 10S rail fragment.

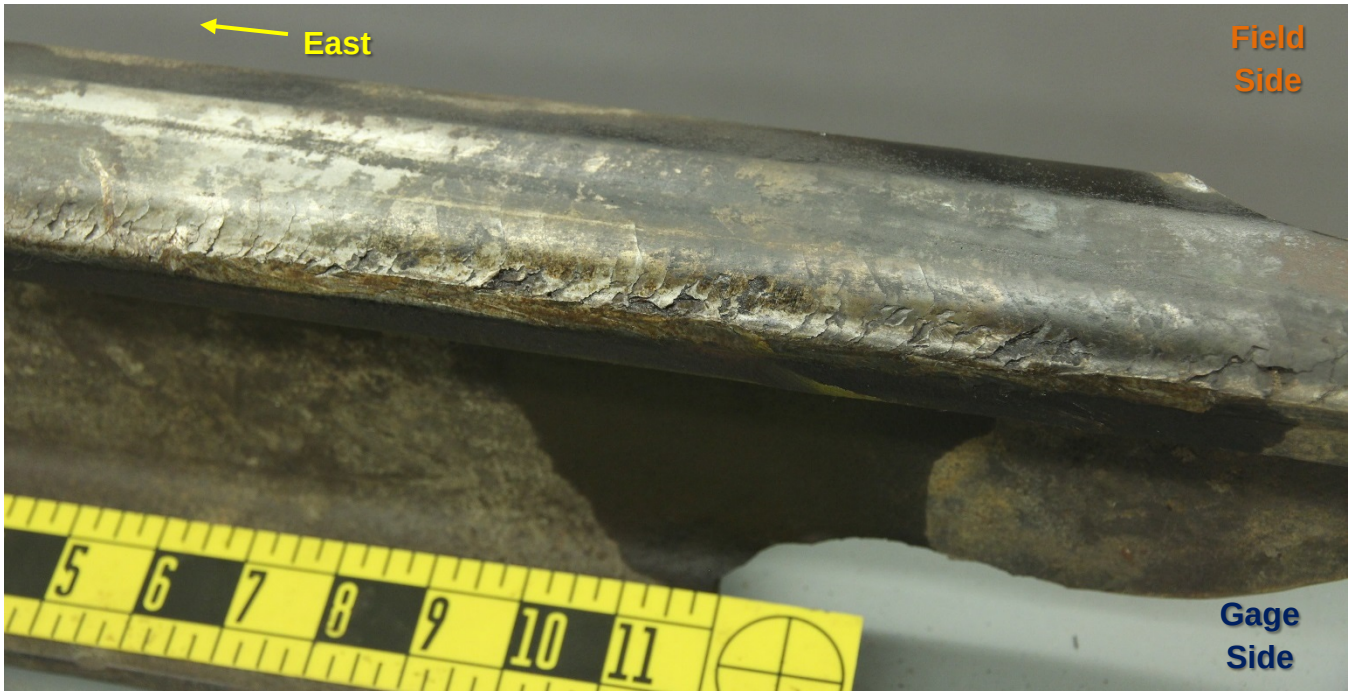

Figure 32 – Closer view of head checking and shelling on the gage side of the 10S fragment.

Figure 33 – The gage side of the west-facing fracture of the 4S rail piece, showing a sawtooth fracture in the web (on-scene photo).

Figure 34 – The middle of the 4S rail piece, showing heat tinting on the head surface (on-scene photo).

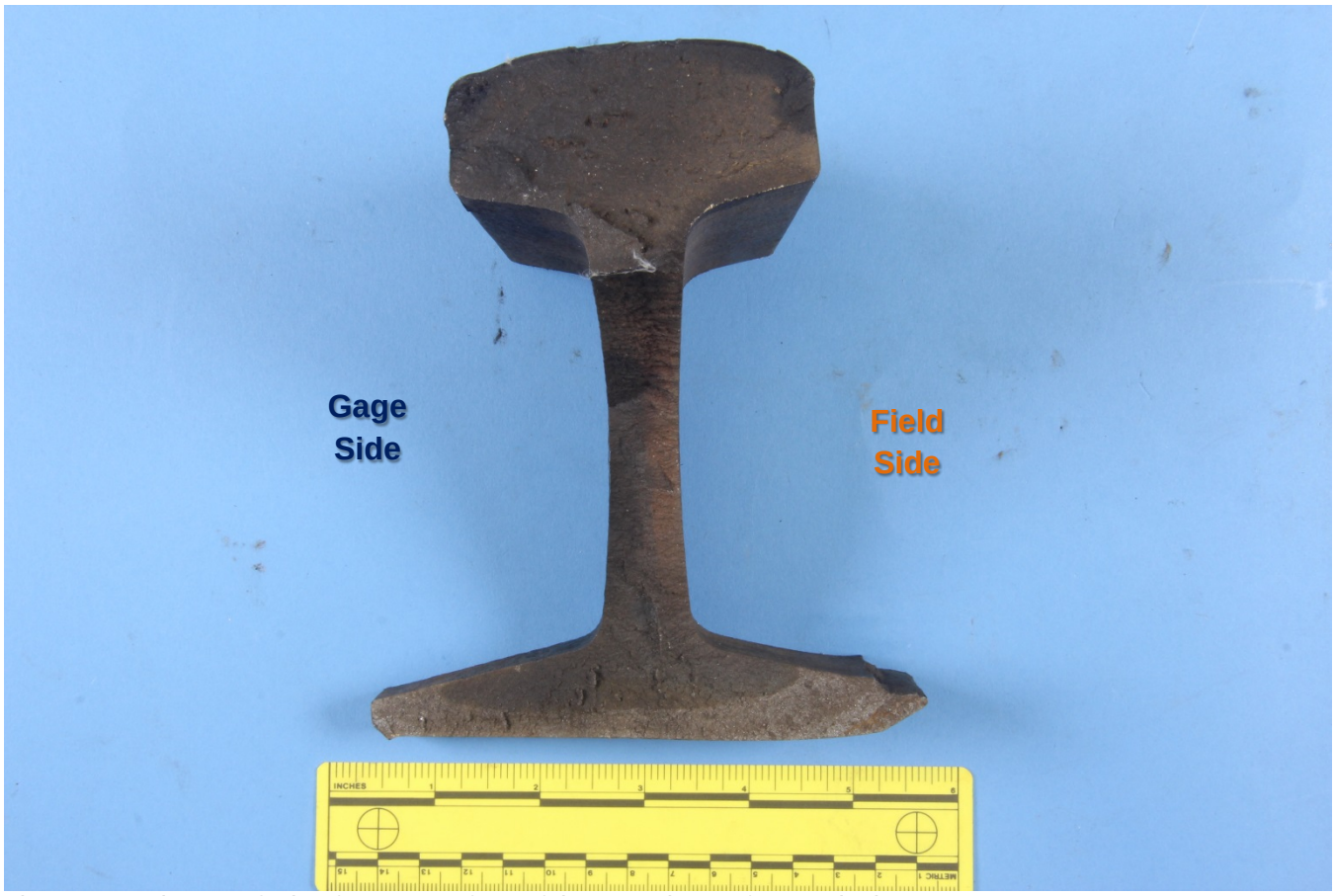

Figure 35 – The east-facing fracture surface of the 10N piece, after sectioning.

Figure 36 – The east-facing 10N fracture surface in Figure 35, after cleaning.

Figure 37 – The 11N fracture surface that mates to the 10N fracture surface in Figure 36, after cleaning.

Figure 38 – Cross section cut of the 10N section of rail.

Figure 39 – Cross section through piece 10N with an outline profile of a new 90-pound rail for reference.

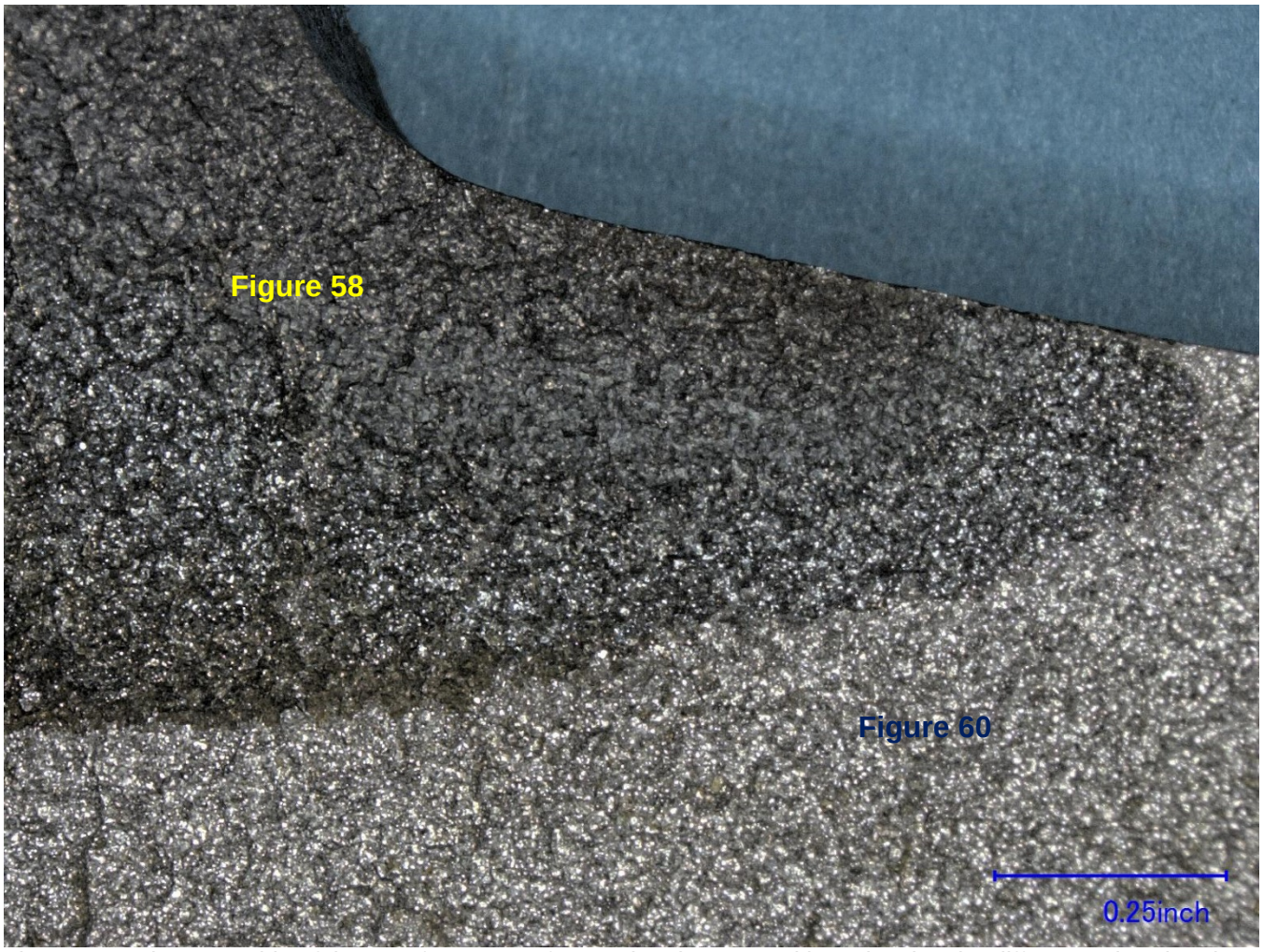

Figure 40 – The gage side of the 10N fracture surface web to base transition, showing the different colored regions of the fracture surface.

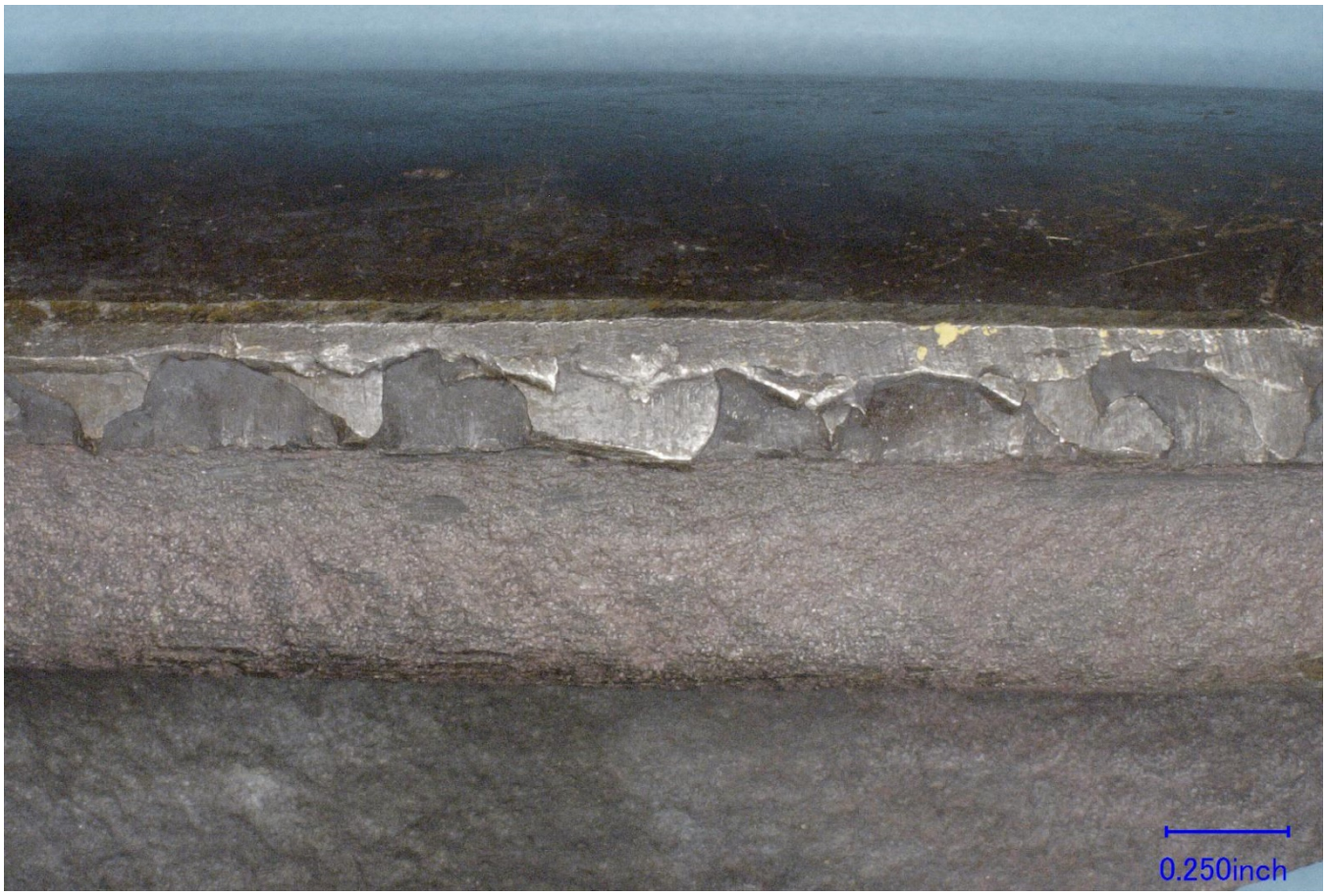

Figure 41 – The gage side of the 10N segment, showing batter consistent with wheel interaction.

Figure 42 – The east-facing fracture face of the 12N rail fragment.

Figure 43 – The east-facing fracture surface on 12N in Figure 42, after cleaning.

Figure 44 – Closer view of the 12N fracture head from Figure 42 after cleaning, showing surface batter.

Figure 45 – View of the east-facing side of the 12N head fracture surface. The boxed area is shown in Figure 46.

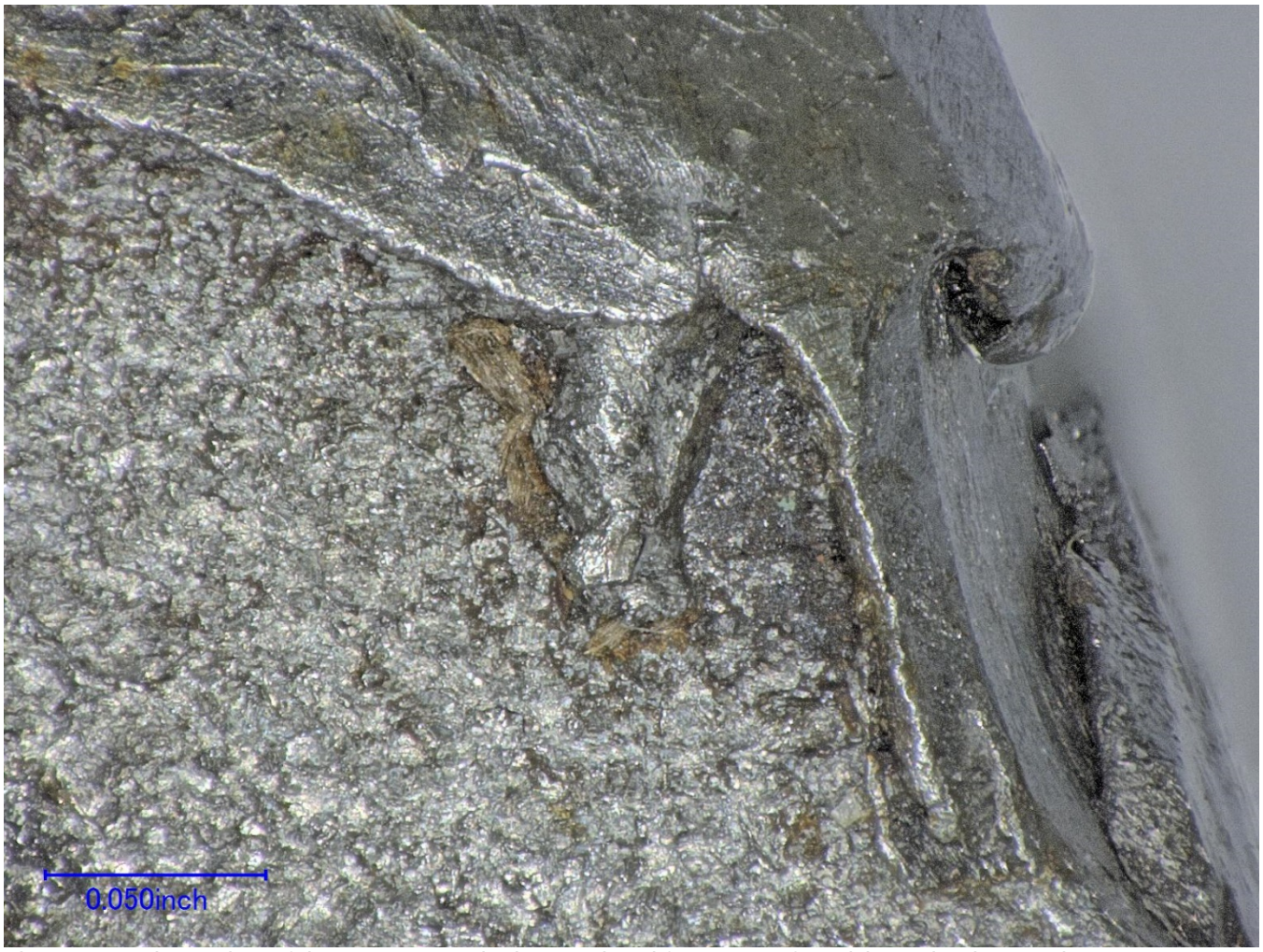

Figure 46 – Closer view of the gage corner in the 12N head fracture surface (shown in Figure 45).

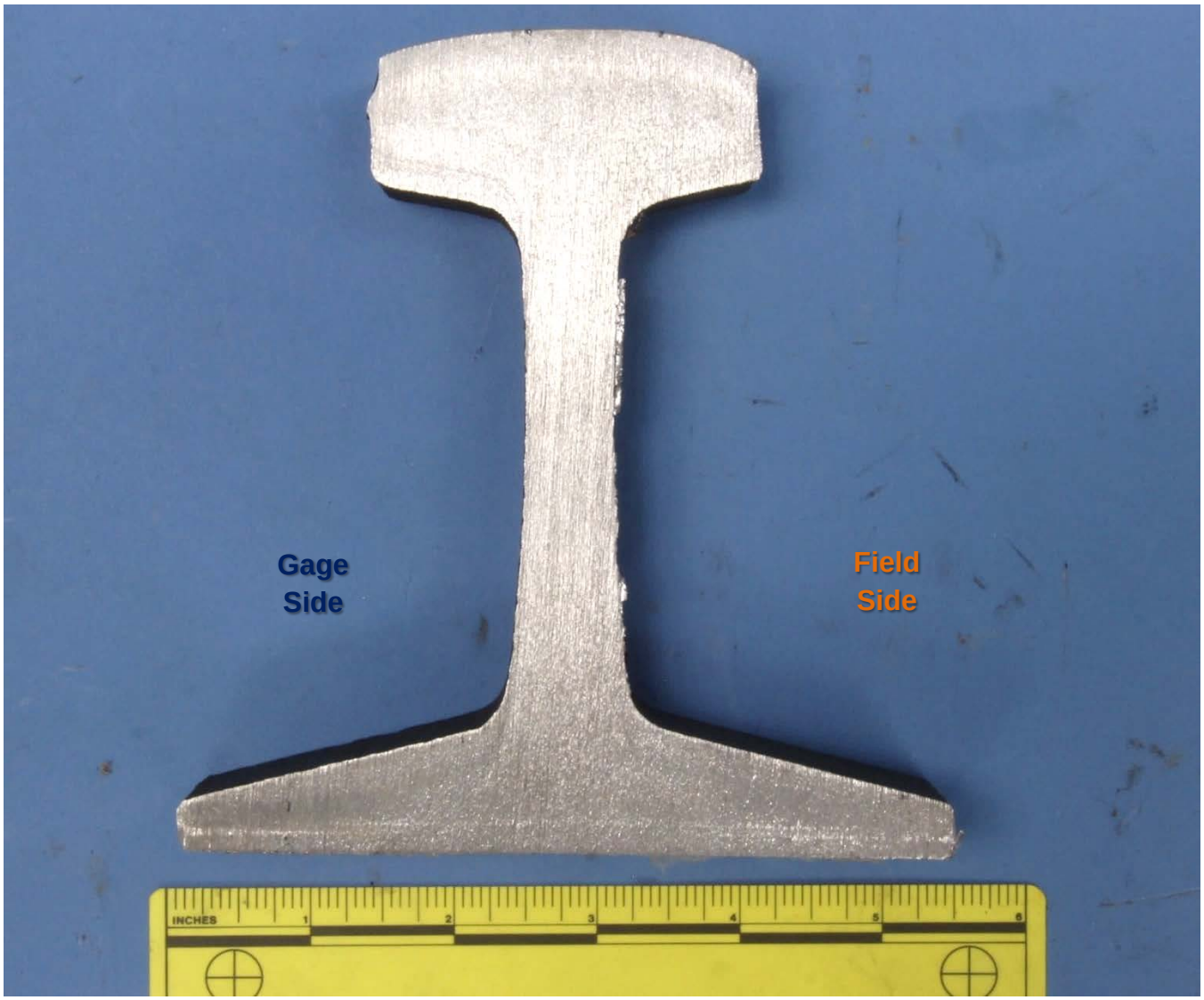

Figure 47 – Cross section cut of the 12N section of rail.

Figure 48 – Cross section through piece 12N with an outline profile of a new 90-pound rail for reference.

Figure 49 – The sectioned east-facing fracture surface of the 10S rail fragment.

Figure 50 – Vertical fracture features on the field side of the east-facing 10S rail fragment fracture.

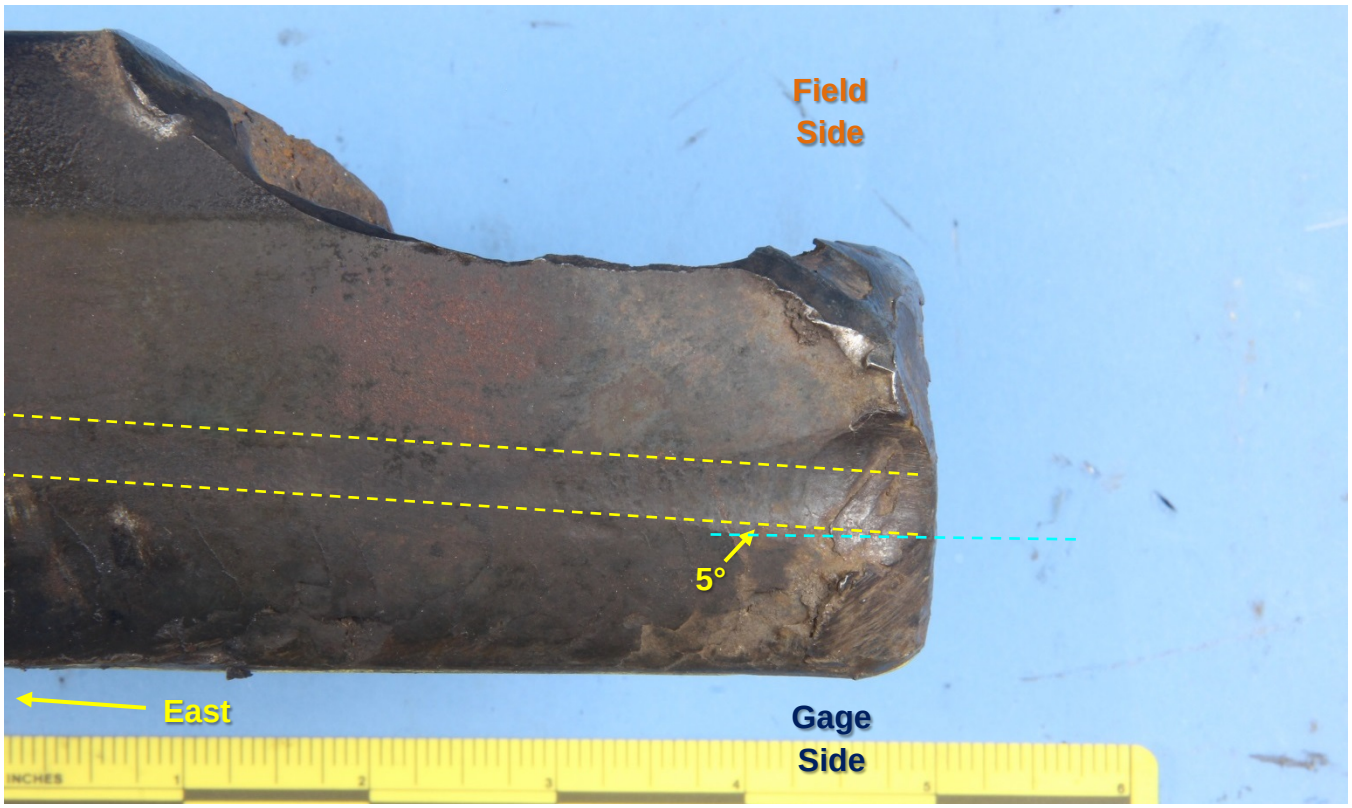

Figure 51 – Top view of the east-facing fracture surface of the 10S rail section. The dashed lines represent the 5° deviation toward the field side.

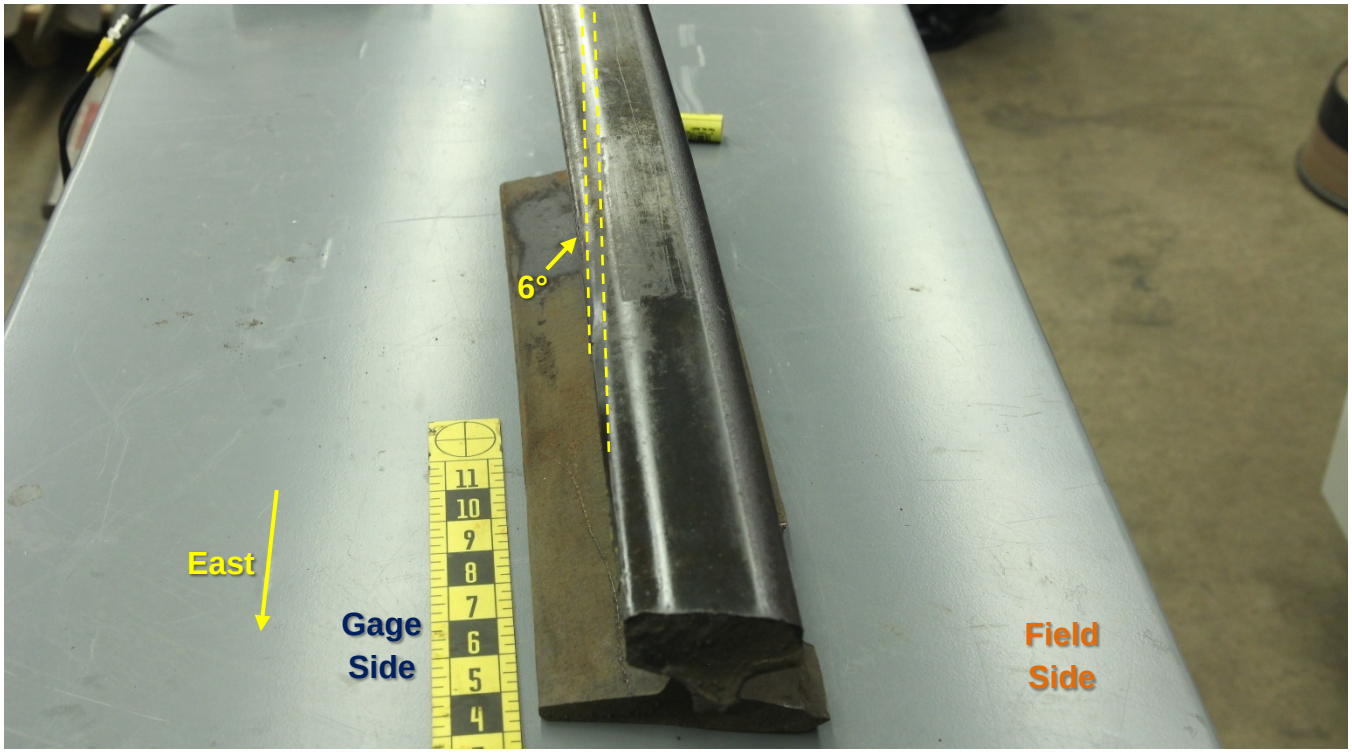

Figure 52 – The east-facing end of the 10N rail fragment. A wheel deviation mark was present on the head running surface, with the angle of departure labeled.

Figure 53 – Closer view of shell cracks of the gage side of the 10S piece.

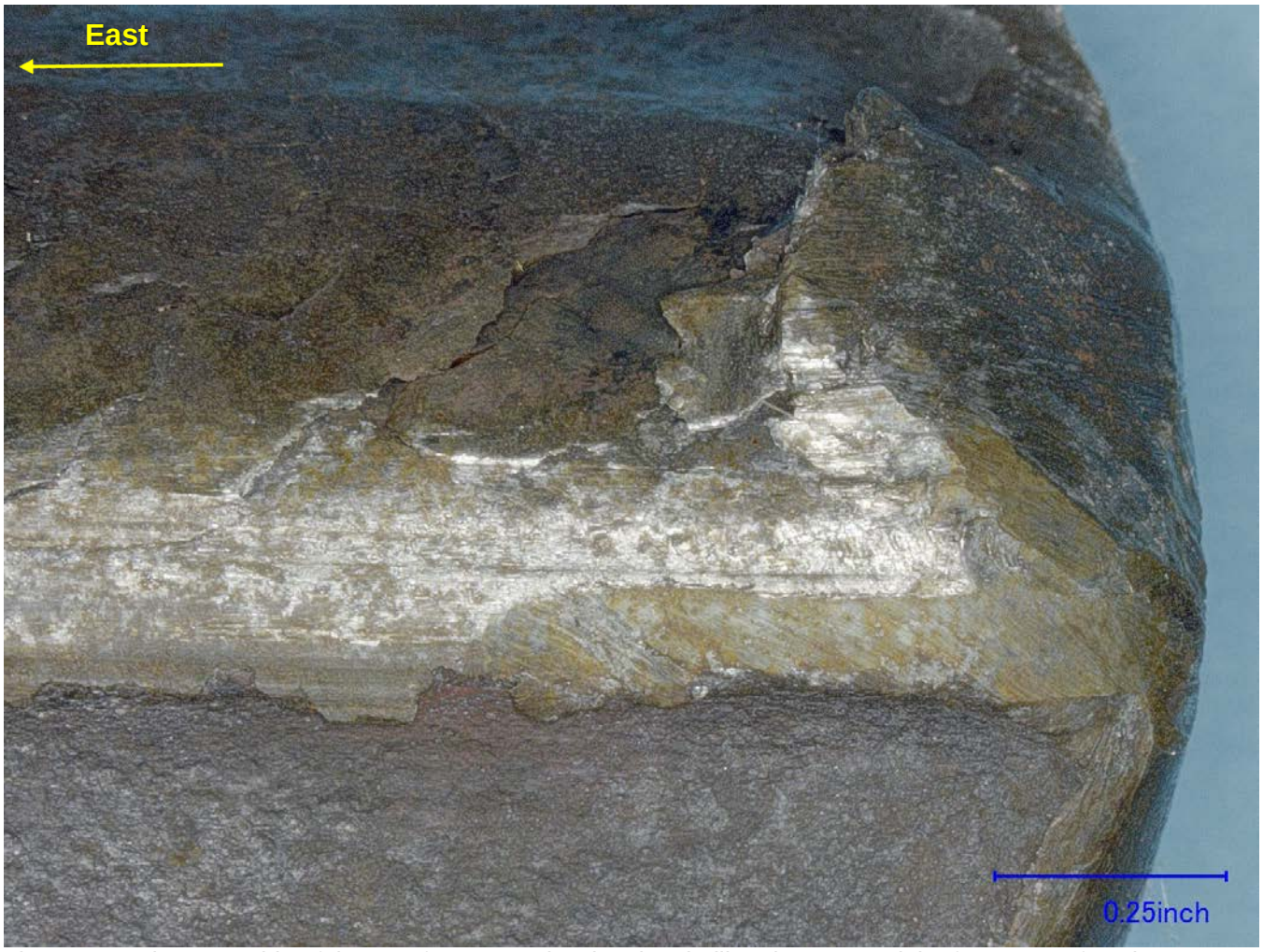

Figure 54 – The gage side of the 10S fragment, showing the shelling damage and the fracture surface batter.

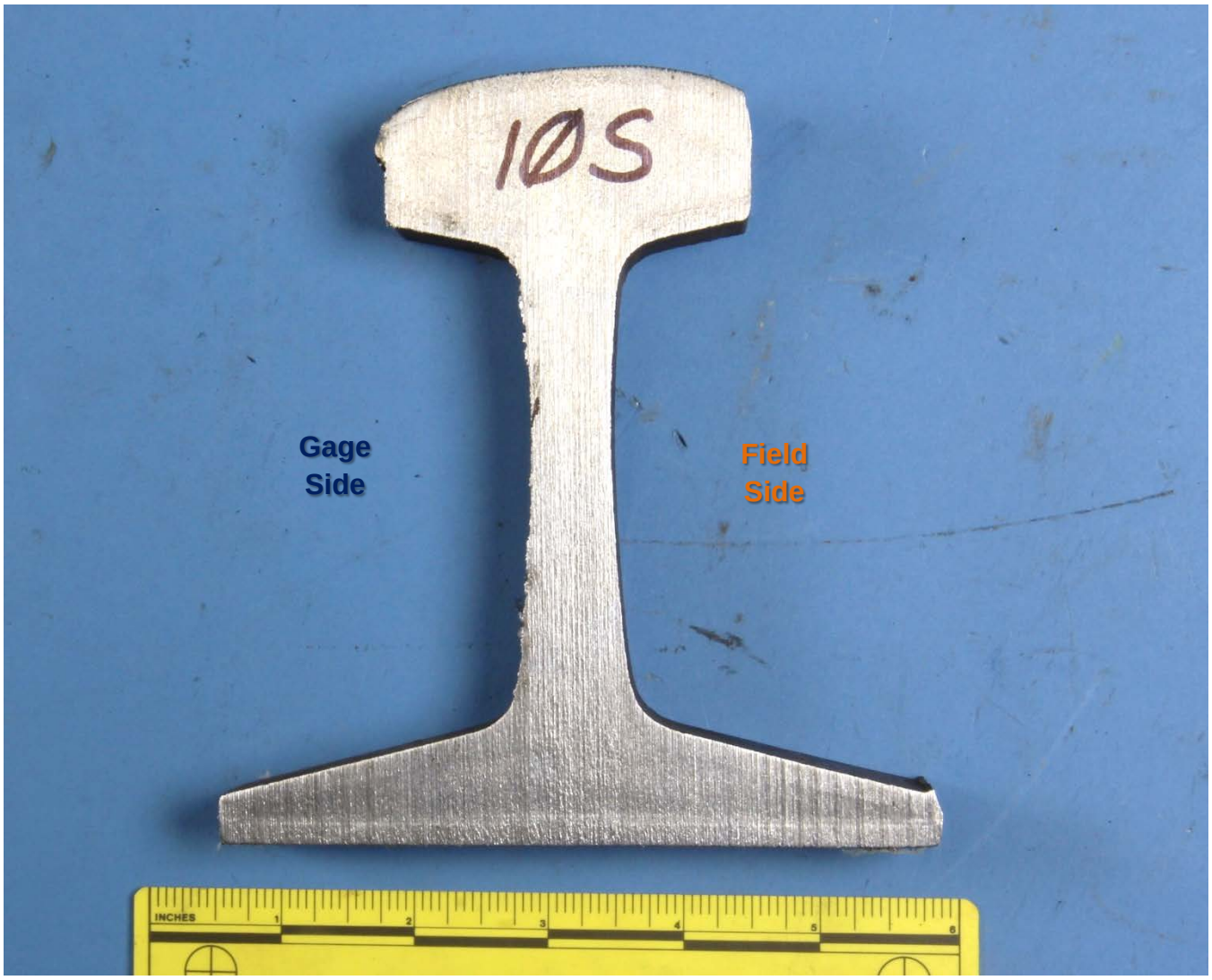

Figure 55 – Cross section of the 10S rail fragment.

Figure 56 – Cross section through piece 10S with an outline profile of a new 90-pound rail for reference.

Figure 57 – Cross section through piece 4S with an outline profile of a new 90-pound rail for reference.

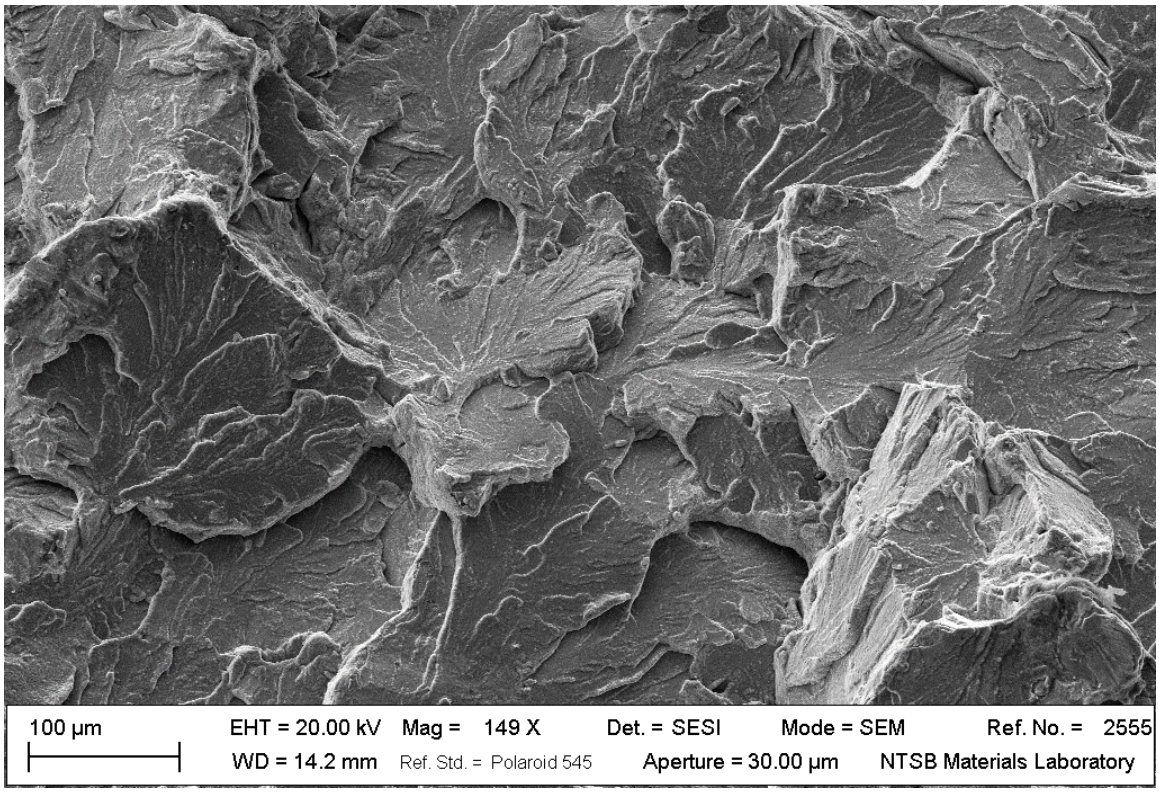

Figure 58 – Secondary electron (SE) micrograph of cleavage facets on the dark part of the fracture surface of 10N.

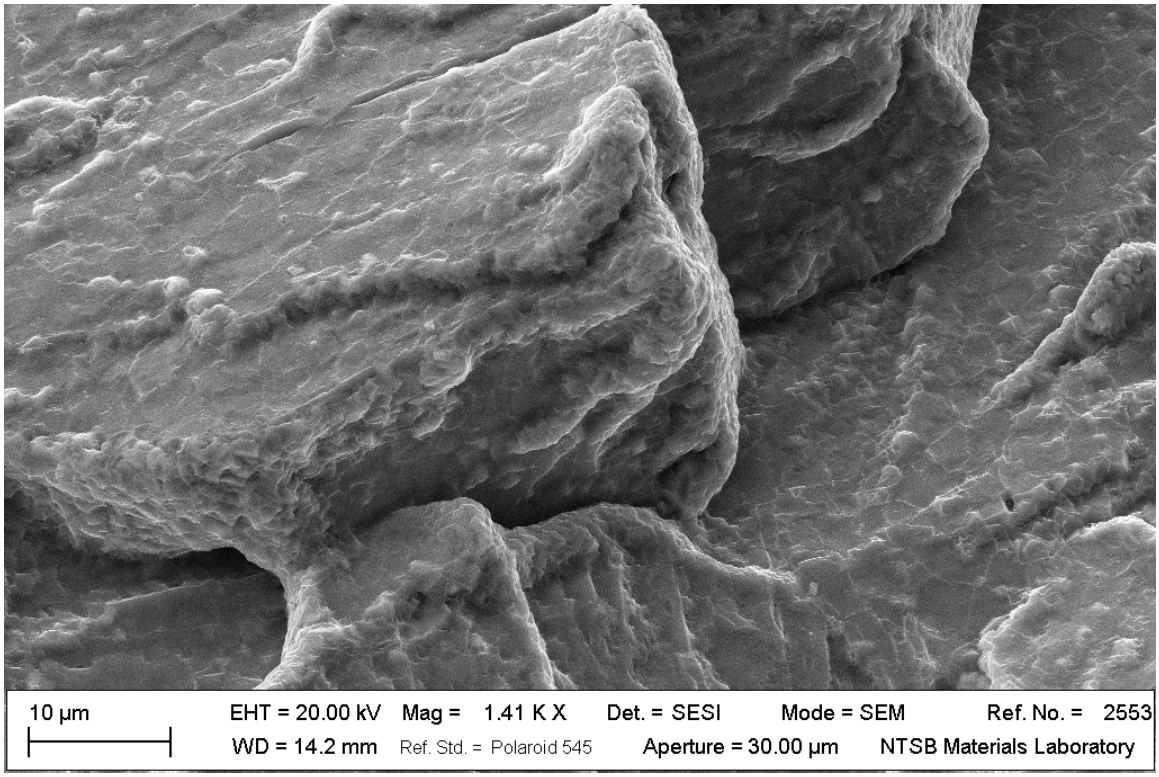

Figure 59 – SE micrograph showing a closer view of Figure 58, showing the rounded surface texture of the facets.

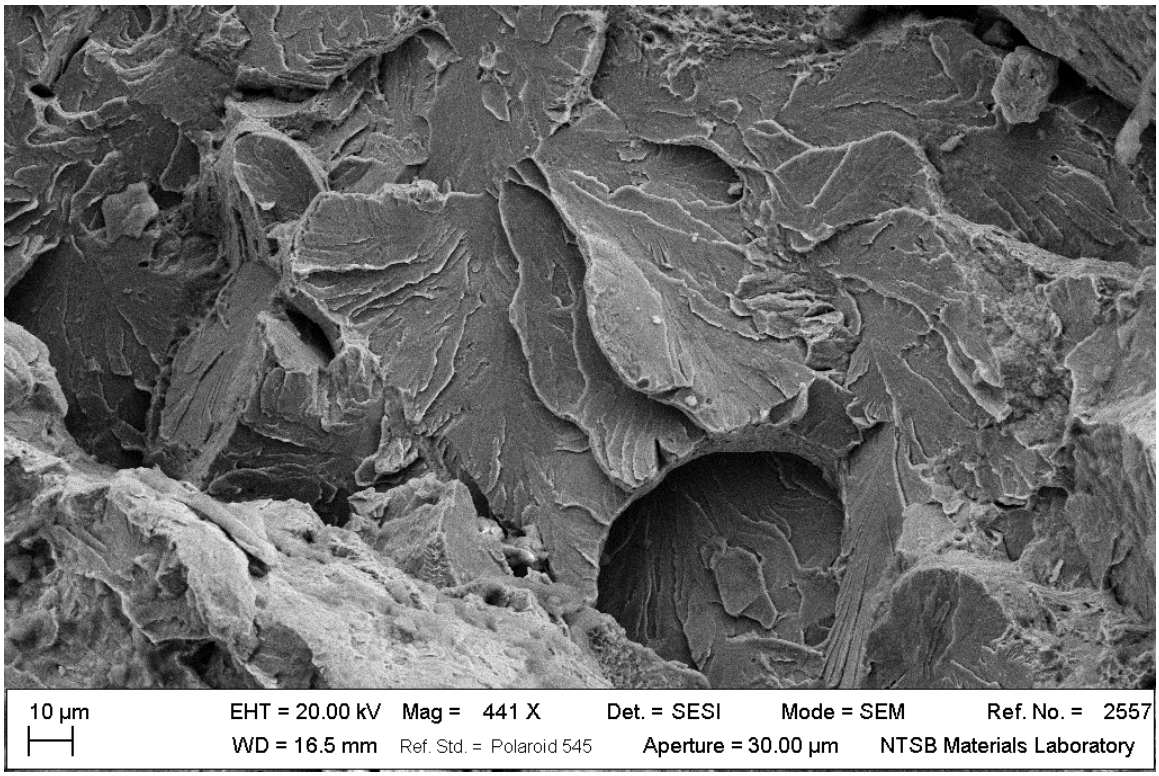

Figure 60 – SE micrograph of the shiny portions of the 10N fracture surface.

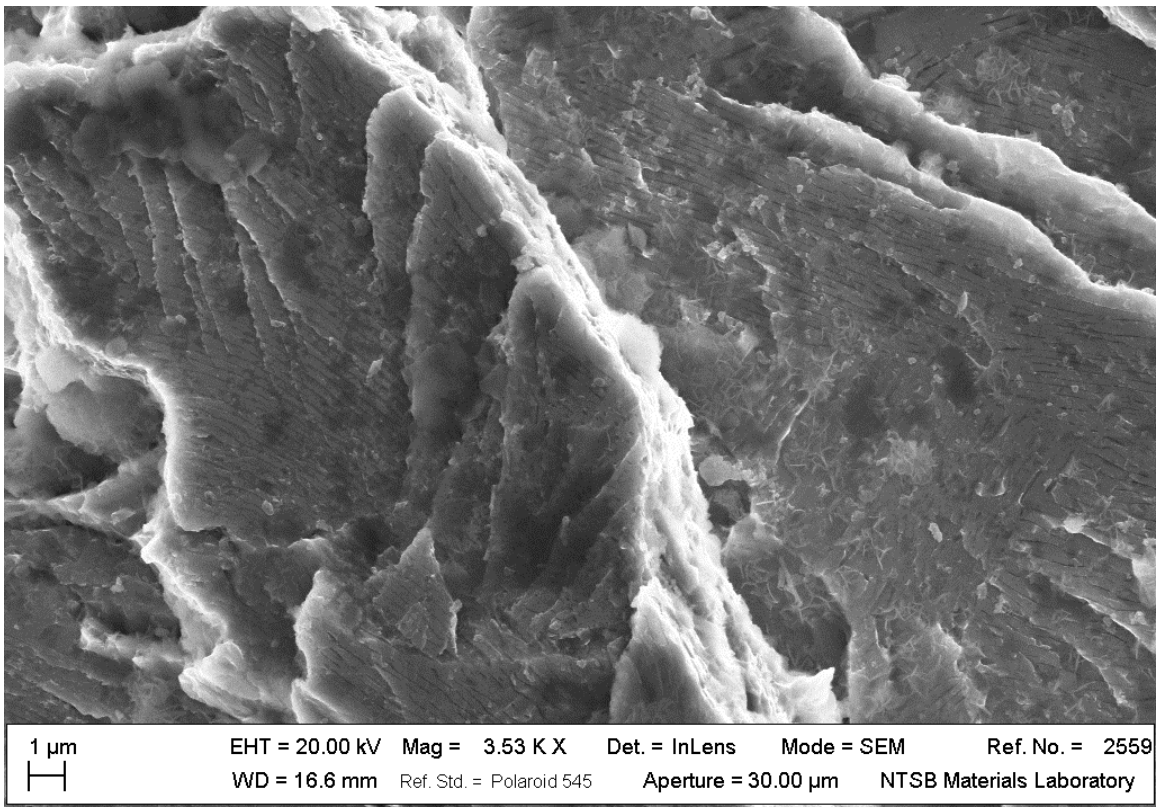

Figure 61 – SE micrograph of a closer view of the cleavage facets with of the shiny fracture surface of 10N.

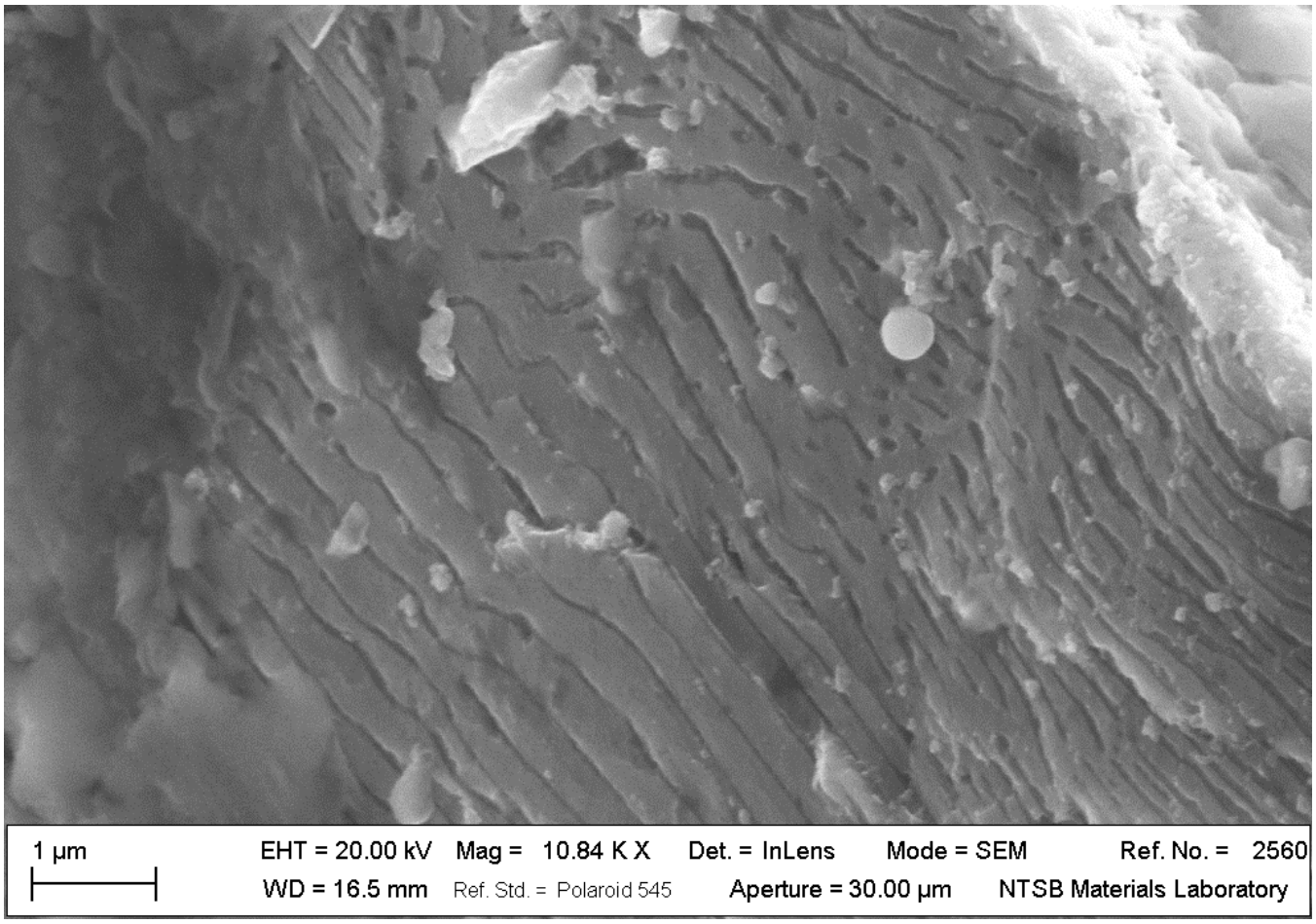

Figure 62 – SE micrograph showing a closer version of the linear features in Figure 61. These features were consistent with the pearlite microstructure (shown in Figure 66).

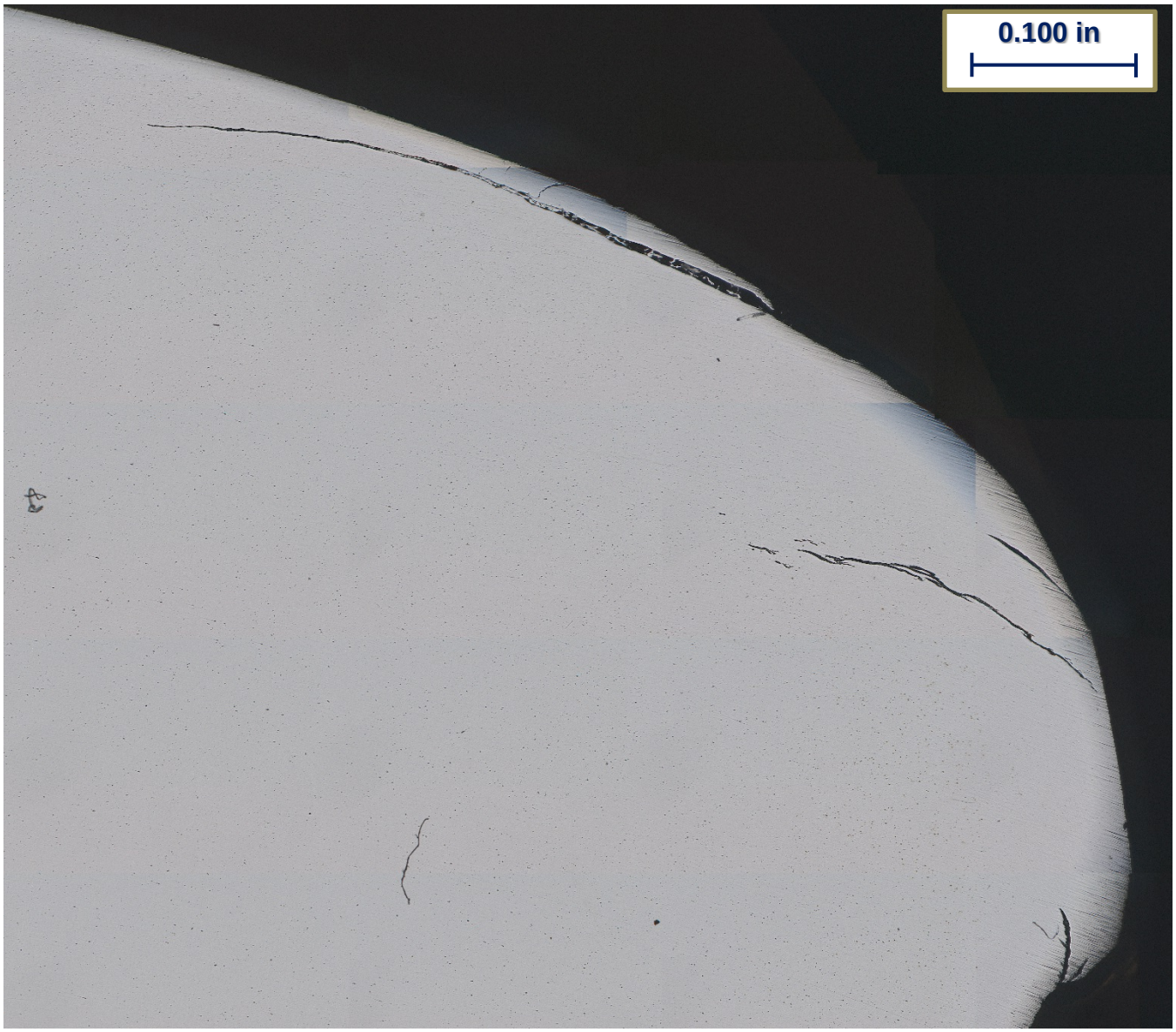

Figure 63 – Bright-field (BF) optical micrograph of a cross section of the 10S head, facing west, as-polished. The gage side is on the right. (~20X).

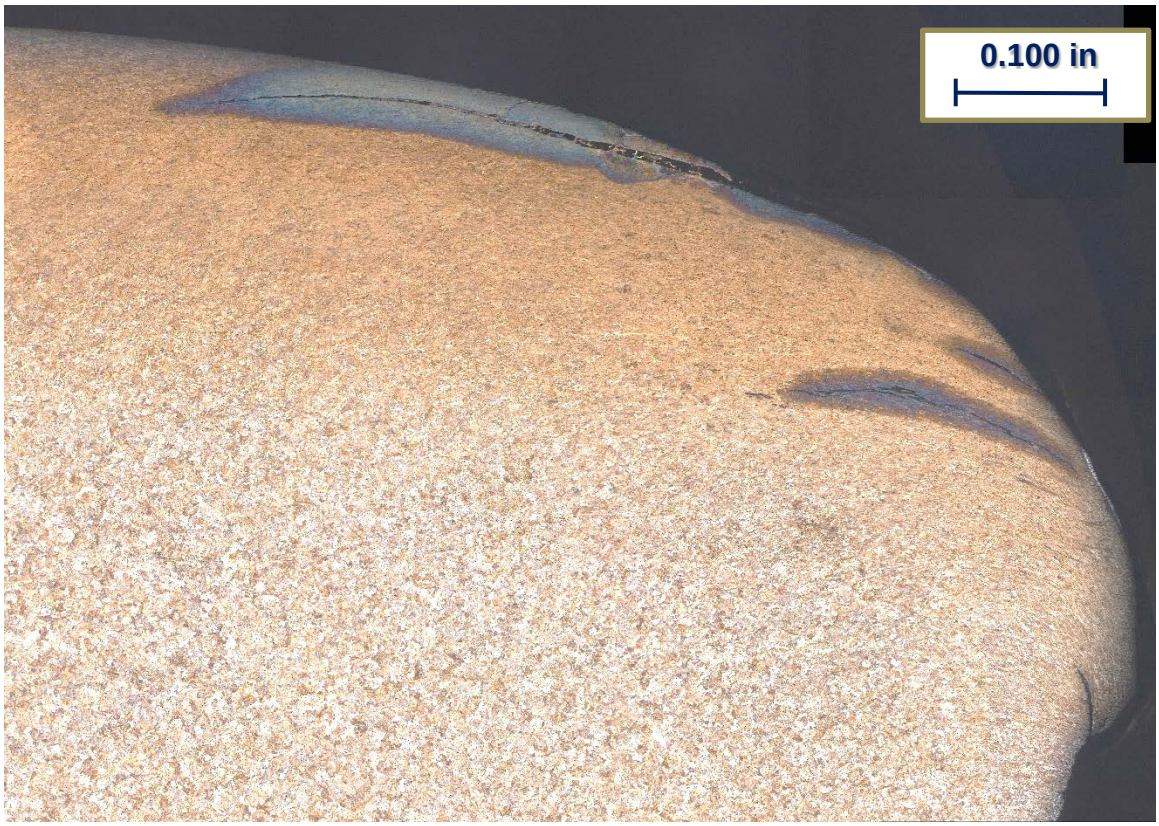

Figure 64 – Bright-field optical micrograph of a cross section of the 10S head, facing west. The gage side is on the right (~20X, etched 2% Nital).

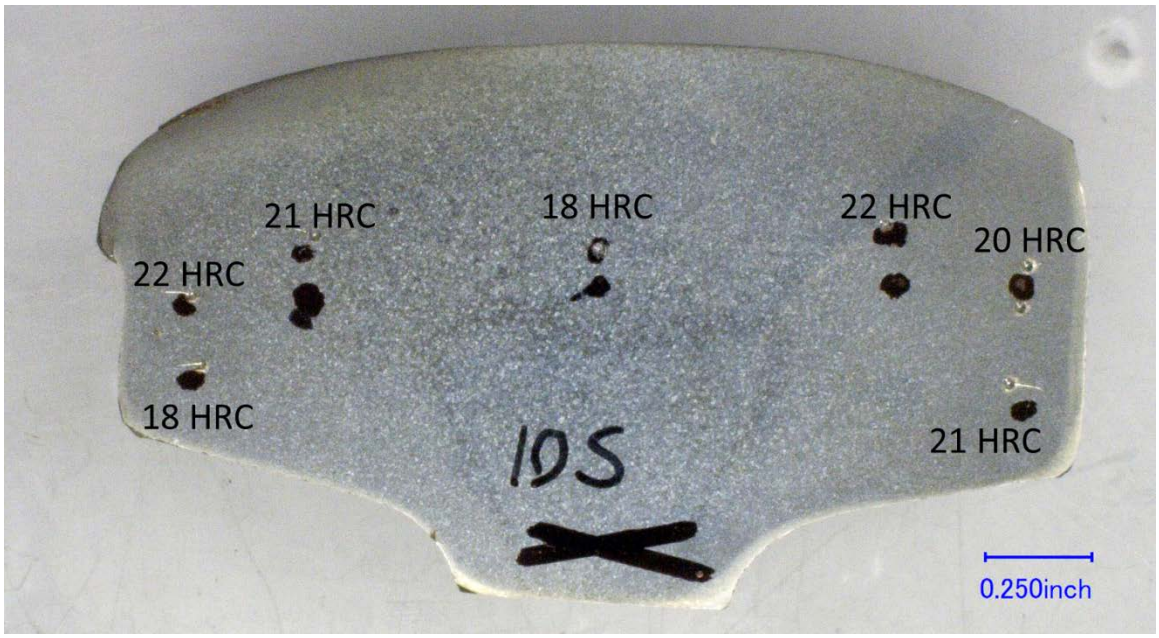

Figure 65 – The polished and etched 10S head, showing Rockwell hardness measurements.

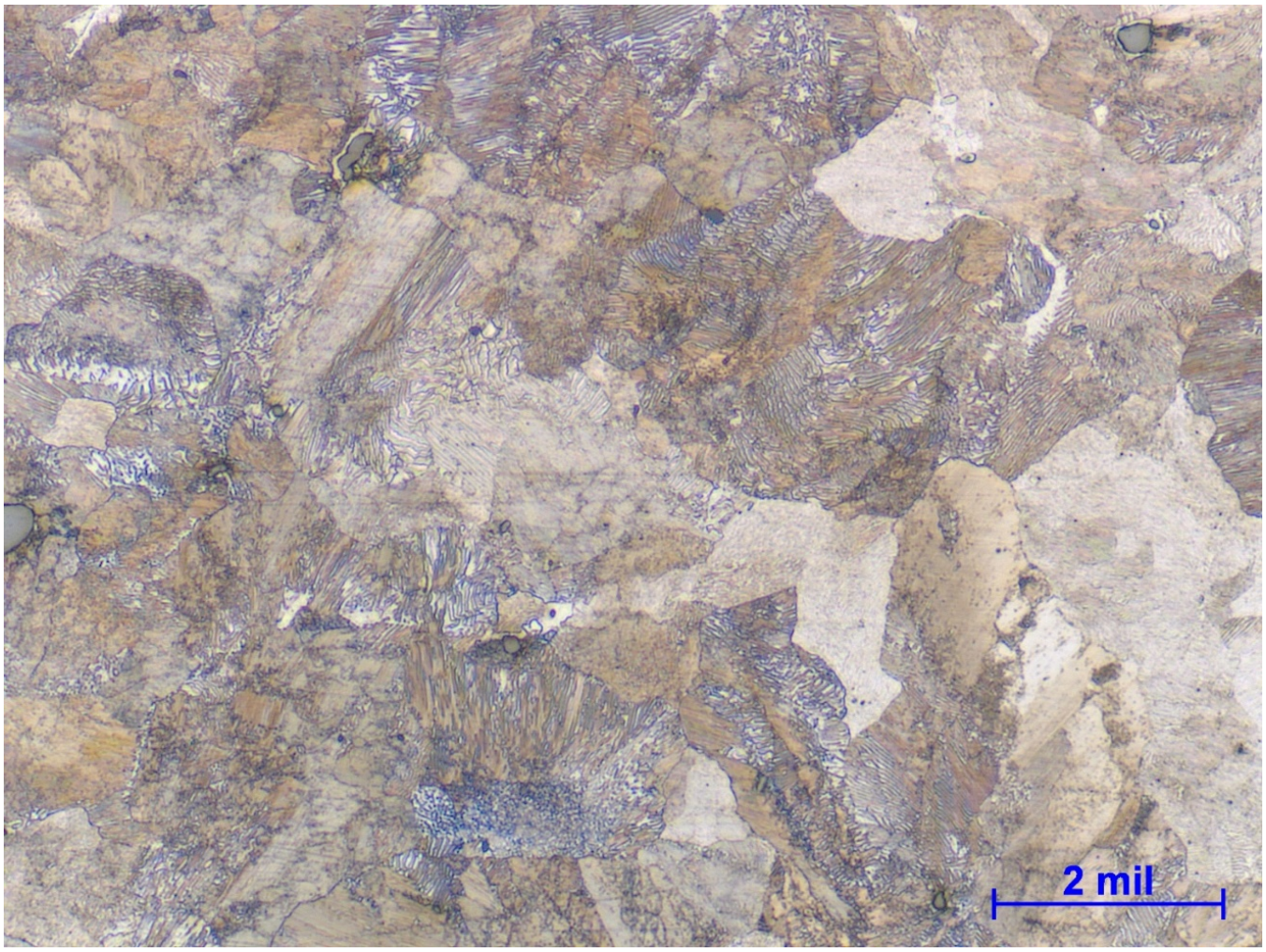

Figure 66 – BF micrograph of the 10S head cross section away from the running surface, showing a microstructure of pearlite and ferrite (~500X, etched 2% Nital).

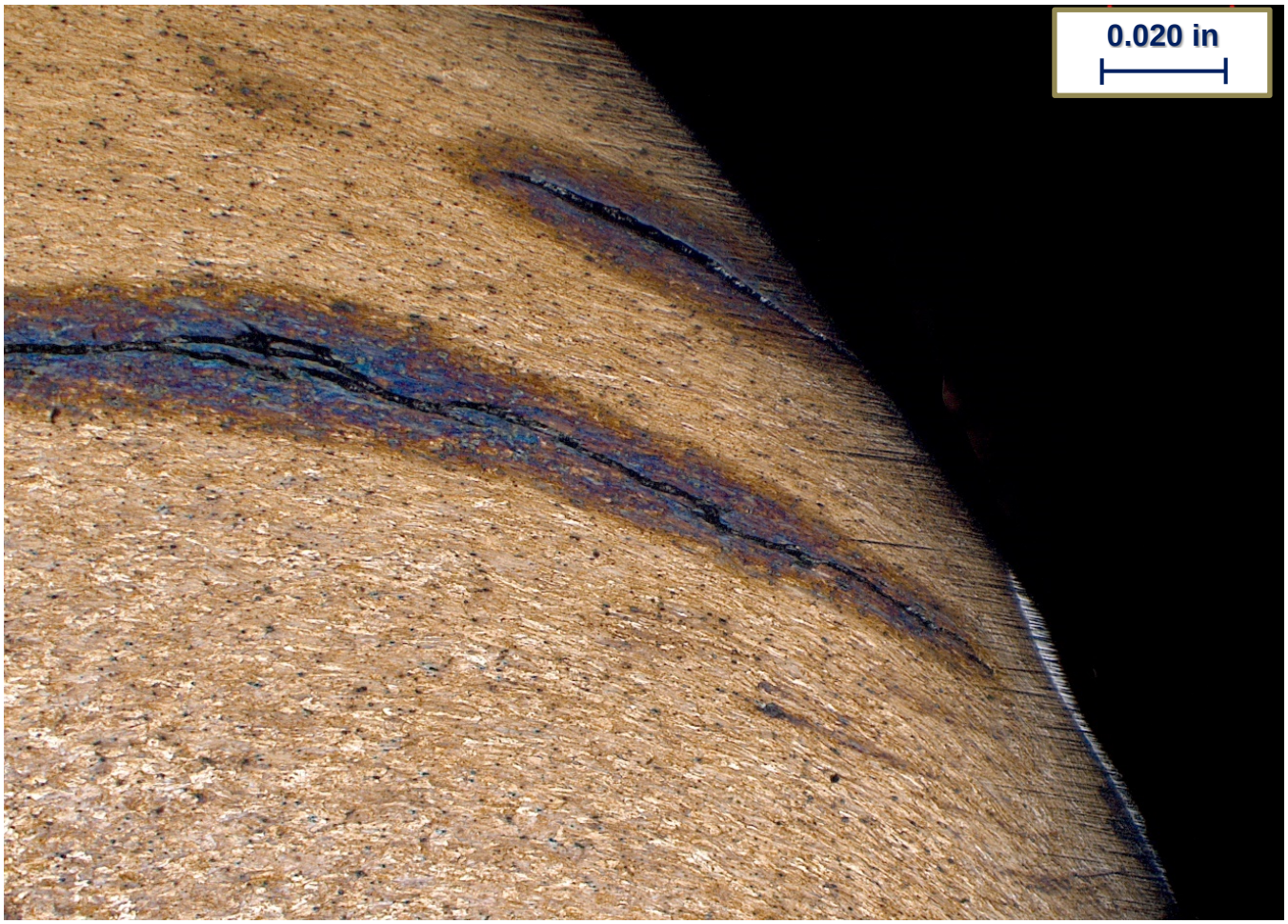

Figure 67 – BF micrograph of the 10S head cross section near the running surface, showing a more compressed grain structure and internal cracks (~500X, etched 2% Nital).

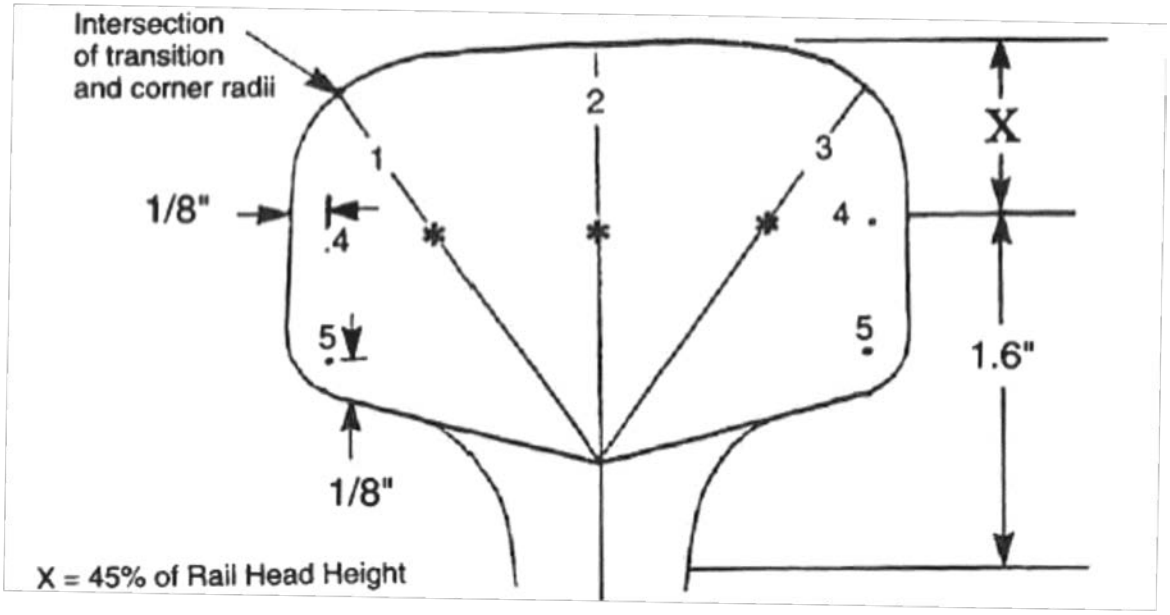

Figure 68 – Diagram showing the seven locations of hardness indents prescribed by AREMA for the determination of internal hardness of cross-sectioned rail heads (courtesy, *AREA Manual for Railway Engineering, Chapter 4: Rail*, (1996) p. 4-2-8)

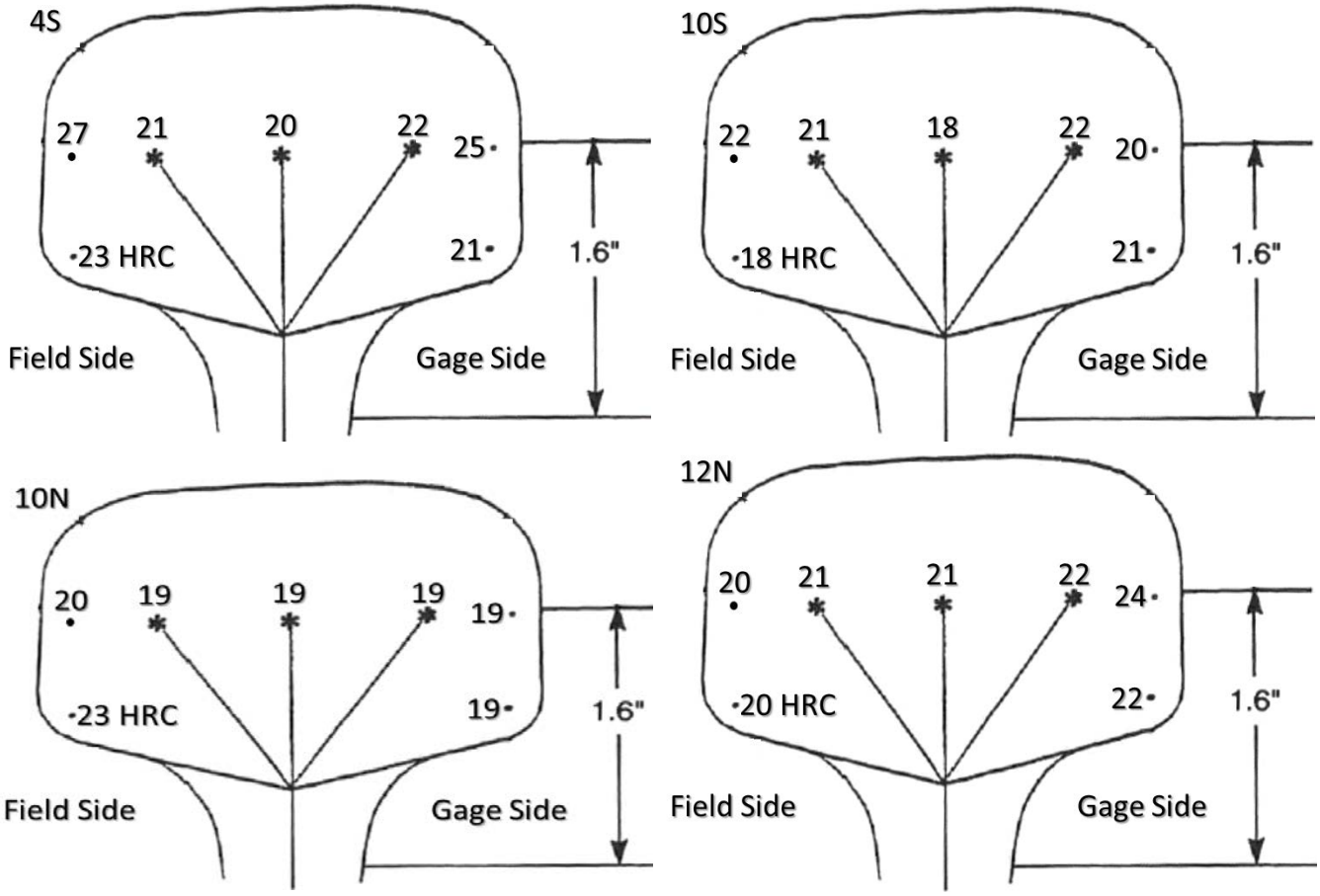

Figure 69 – Diagram of Rockwell hardness results for the cross-sectioned rail heads of 4S, 10S, 10N, and 12N. All results reported in the HRC scale.